Co-funded by the Erasmus+ Programme of the European Union

BRIGHT

Erasmus+ strategic partnership for Higher Education

BOOSTING THE SCIENTIFIC EXCELLENCE AND INNOVATION CAPACITY OF 3D PRINTING METHODS IN PANDEMIC PERIOD

MODULE 3

Material Science & Strength of Materials

Project Title	**Boosting the scientific excellence and innovation capacity of 3D printing methods in pandemic period 2020-1-RO01-KA226-HE-095517**
Output	**O1 - BRIGHT e-learning support courses for curriculum aiming to boost the scientific excellence and innovation of 3D printing methods used for developing and producing medical parts in pandemic period**
Module	**Module 3 Material Science & Strength of Materials**
Date of Delivery	**July 2021**
Authors	**Remigiusz ŁABUDZKI Radosław WICHNIAREK Filip SARBINOWSKI Sven MARIČIĆ**
Version	**FINAL VARIANT**

This project has been funded with support from the European Commission. This publication [communication] reflects the views only of the authors, and the Commission cannot be held responsible for any use which may be made of the information contained therein.

Contents

This project has been funded with support from the European Commission. This publication [communication] reflects the views only of the authors, and the Commission cannot be held responsible for any use which may be made of the information contained therein.

This project has been funded with support from the European Commission. This publication [communication] reflects the views only of the authors, and the Commission cannot be held responsible for any use which may be made of the information contained therein.

1 Introduction

Biomaterials rapid prototyping (RP), recently known as additive manufacturing (AM), has appeared as a revolutionary technology, promising to transform research into medical therapeutics. RP is a layer by layer manufacturing process which directly translates computer data such as Computer Aided Design (CAD), Computer Tomography (CT), and Magnetic Resonance Imaging (MRI) into three-dimensional (3D) objects. RP technologies play a significant role in biomedical industry such as anatomical models for surgery training/planning, rehabilitation, dentistry, customized implants, drug delivery devices, tissue engineering, and organ printing. The integration of biomaterials and rapid prototyping technologies is an exciting route in developing biomaterial implants for the past decade. This review describes and classifies the RP systems into three categories of liquid-based, solid-based, and powder-based according to the initial form of their feed materials. Then, discusses possible benefits, drawbacks, and applications of each process in the field of biomaterials science and engineering.

Chapter 2 presents an overview of the known and most important additive manufacturing techniques in terms of materials engineering.

Chapter 3 discusses the basic definitions and research techniques in the field of material strength.

Chapter 4 presents examples of non-destructive research techniques for optical and electron microscopy.

Chapter 5 gives an example of an orthosis strength analysis.

This project has been funded with support from the European Commission. This publication [communication] reflects the views only of the authors, and the Commission cannot be held responsible for any use which may be made of the information contained therein.

2 Materials for 3D printing – review known techniques

RP systems will likely require a variety of biomaterials, cellular and acellular, in terms of maintaining both cell-compatibility and printability. Using of 3D printed surgical aids and implants, directly 3D printed or shaped based on 3D printed plastic or resin models, is becoming commonplace for orthopedics, craniofacial reconstruction, plastic surgery, and dental and oral applications. RP systems are classified broadly into three categories of liquid-based, solid-based, and powder-based depend on the initial form of its material which can be various polymers, ceramics and metals and composites. Figure 1.1 shows the classification of RP techniques.

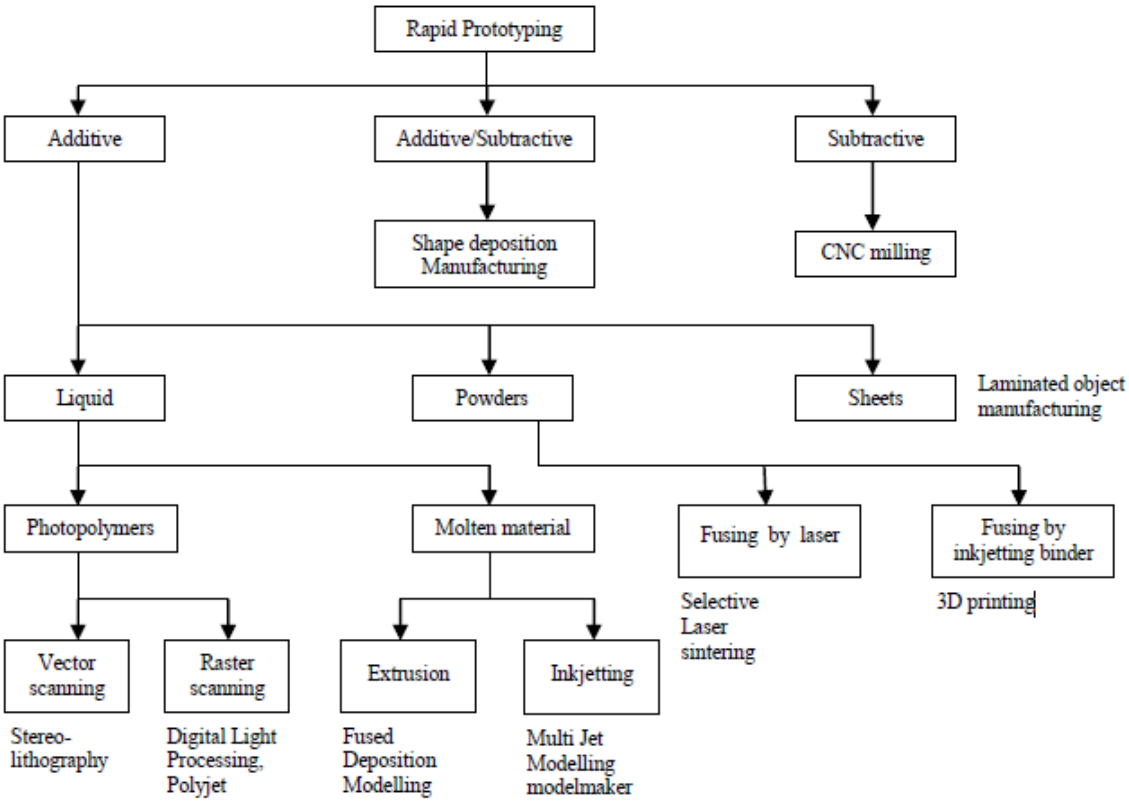

Fig. 1.1. Classification of RP methods [1]

2.1 Biomedical requirement of rapid prototyping

Rapid Prototyping decreases development time by allowing corrections to a product to be made early in the process. By giving engineering and medical surgeons to look at the product early in the design process, mistakes can be corrected and changes can be made while they are still inexpensive. The trends in development continue to emphasize the following [2]:

- Increasing number of variants of products.
- Increasing product complexity.

This project has been funded with support from the European Commission. This publication [communication] reflects the views only of the authors, and the Commission cannot be held responsible for any use which may be made of the information contained therein.

• Decreasing product lifetime before obsolescence.

• Decreasing delivery time

The use of RP technology has been slow arriving in the medical arena, the potential of the technique is seen to be widespread. Various uses of the technology within surgical planning, prosthesis development and bioengineering are discussed. Some possible drawbacks are noted in some applications, owing to the poor resolution of CT slice data in comparison with that available on RP machines, but overall, the methods are seen to be beneficial in all areas, with one early report suggesting large improvements in measurement and diagnostic accuracy as a result of using RP models [3].

Rapid prototyping (RP) has become a widely used tool for the fabrication and evaluation of physical prototypes during the product development cycle. RP is used since it can produce prototypes with arbitrary shapes quickly and at a lower cost than traditional prototyping techniques. Recently RP has also been investigated regarding its ability to replace traditional mass manufacturing processes in applications where only one or a small number of individually shaped parts are required. There are some reasons to use RP which are as follows [4]:

• To increase effective communication.

• To decrease development time.

• To decrease costly mistakes.

• To minimize sustaining engineering changes.

• To extend product lifetime by adding necessary features and eliminating redundant features early in the design.

There are varieties of materials which can be used for medical applications of RP. Which material should be selected depends on the purpose of made model (planning procedures, implants, prostheses, surgical tools, and tissue scaffold), demanded properties of material for concrete application and the possibilities of the chosen RP technique. Materials must show biological compatibility. RP medical materials include [5]:

• Photosensitive resins for medical application;

• Metals (stainless steel, titanium alloys, Cobalt Chromium alloys, other);

• Advanced bioceramic materials (Alumnia, Zirconia, Calcium phosphate-based bioceramics, porous ceramics) for LOM;

• Polycaprolactone (PCL) scaffolds, polymer-ceramic composite scaffold made of polypropylene-tricalcium phosphate (PP-TCP). PCL and PCL-hydroxyapatite (HA) for FDM, PLGA, starch-based polymer for 3DP, polyetheretherketone-hydroxyapatite (PEEK-HA), PCL scaffolds in tissue engineering for (SLS);

• Bone cement: new calcium phosphate powder binders (mixture of tetracalcium phosphate (TTCP) and beta – tricalcium phosphate (TCP)), Polimethyl methacrylate (PMMA) material, other polymer calcium phosphate cement composites for bone substitutes and implants;

• Many other biocompatible materials.

This project has been funded with support from the European Commission. This publication [communication] reflects the views only of the authors, and the Commission cannot be held responsible for any use which may be made of the information contained therein.

2.2 *Biomaterials in RP applications*

2.2.1 Surgery

The most important dysmorphies in CMF surgery are congenital, system-bound growth disorders, facial craniosynostoses, like M.Crouzon, Apert-syndrome, Bindersyndrome, and other congenital skull and face dysplasiae, like the Frachescetti-syndrome, Pierre-Robin-syndrome, or hemifacial microsomia. Due to the high variability in the expression of these dimorphisms and due to the extreme complexity of craniofacial operations, the first 3D reproductions were developed some years ago especially for facial surgery. The 3D model is often superior to a mere 3D visualization because it enables the surgeon to answer important questions during the surgical simulation that define the intervention strategy and minimize the need for ad-hoc decisions to circumvent unexpected intraoperative problems. Many surgical questions can be answered based on the RP model and the simulation performed on it. Among these are information on the extent of translations, rotations, advancements and fixability of dissected bone segments, whether autogenous bone transplants will be needed, whether defects will be coverable by autogenous or allogenous material, what osteosynthesis material is optimally suited, and so on.

Ossiculoplasty is a technique for reconstruction of the ossicles within the middle ear for improved hearing . The malleus, incus, and stapes bones serve to transmit incoming sounds from the tympanic membrane to the inner ear.

Materials used in ossicular replacement prostheses must demonstrate appropriate biological compatibility, acoustic transmission, stability, and stiffness properties. Prostheses prepared using Teflon, titanium, Ceravital and other conventional materials have demonstrated several problems, including migration, perforation of the tympanic membrane, difficulty in shaping the prostheses, and reactivity with the surrounding tissues. The two-photon polymerization for rapid prototyping of Ormocer1 middle-ear bone replacement prostheses. Ormocer1 surfaces fabricated using two-photon polymerization exhibited acceptable cell viability and cell growth profiles. The Ormocer prosthesis was able to be inserted and removed from the site of use in the frozen human head without fracture. The two-photon polymerization is able to create ossicular replacement prostheses and other medical devices with a larger range of sizes, shapes and materials than other micro fabrication techniques.

Stereo lithography is particularly versatile with respect to the freedom of designing structures and the scales at which these can be built: submicron-sized structures as well as decimetre-sized objects have been fabricated. In the biomedical field, these developments have led to the fabrication of patient-specific models for mould assisted implant fabrication, aids for complex surgery and tailor made parts such as hearing aids. More recently, biodegradable materials have been developed for the preparation of medical implants, such as tissue engineering scaffolds by stereo lithography. In implantations using drill guides built by stereo lithography, the accuracy of the implantation was much improved when compared to using conventional surgical guides, particularly in oral surgery [6].

This project has been funded with support from the European Commission. This publication [communication] reflects the views only of the authors, and the Commission cannot be held responsible for any use which may be made of the information contained therein.

Stereo lithography has been also used to fabricate moulds for the preparation of implants in cranial surgery; using data from CT scans [7].

Bio printing technology has emerged as a powerful tool for building tissue and organ structures in the field of tissue engineering. This technology allows precise placement of cells, biomaterials and bio molecules in spatially predefined locations within confined three-dimensional (3D) structures. Various bio printing technologies have been developed and utilized for applications in life sciences, ranging from studying cellular mechanisms to constructing tissues and organs for implantation, including heart valve, myocardial tissue, trachea and blood vessels. Bio printing technology has gained enormous attention as a fabrication methodology for producing 3D structures. Multiple cells, biomaterials and biological molecules can be printed simultaneously in defined spatial locations, yet many challenges remain for building complex tissues consisting of multiple cell types in a confined micro architecture.

More importantly, hydrogel development, resolution enhancement and vascularisation are necessary to apply bio printing technology clinically [8].

2.2.2 Orthopaedics

Orthopaedics is the medical area where application of the biomaterials is highly developed both for commercialization and research purpose. The need for new materials in orthopaedic surgery arises from the recognition of the stress-shielding effect of bone by high-modulus implants presently made of engineering alloys. A lower modulus implant material will result in the construction of a more biomechanically compatible prosthesis. In this respect, composite materials are gaining importance because they offer the potential for implants with tailormade stiffness in contrast to metals.

One of the main issues in orthopaedic implant design is the fabrication of scaffolds that closely mimic the biomechanical properties of the surrounding bone. It is reported on a multi-stage rapid prototyping technique that was successfully developed to produce porous titanium scaffolds with fully interconnected pore networks and reproducible porosity and pore size. The scaffolds porous characteristics were governed by a sacrificial wax template, fabricated using a commercial 3D-printer. Powder metallurgy processes were employed to generate the titanium scaffolds by filling around the wax template with titanium slurry. The porous titanium scaffolds have the properties to be potentially employed in orthopaedic applications. A porous titanium scaffold with controlled porous structure and high strength has been created using a combination of RP and PM techniques. A wax model, created using a commercial 3D-printer, provided the template for the porous titanium scaffold. Characteristics of the PM process, such as titanium slurry concentration, compaction pressure, and sintering temperature, were found to influence the structure and strength of the scaffolds [9].

The unique combination of low stiffness, high strength, high recoverable strains and large energy absorption of porous super elastic NiTi, together with the known biocompatibility of NiTi, makes this material attractive for bone– implant applications. The interest in using porous materials for orthopaedic reconstructive surgery as a means of replacing autografts is of increasing interest and the

This project has been funded with support from the European Commission. This publication [communication] reflects the views only of the authors, and the Commission cannot be held responsible for any use which may be made of the information contained therein.

large number of scientific reports confirm this trend. For loadbearing orthopaedic applications, metals have so far shown the greatest potential as the basis for such scaffolds, owing to their excellent mechanical strength and resilience when compared to alternative biomaterials, such as polymers and ceramics. The focus thereby has mainly been on applications that involve bone ingrowth into the porous scaffolds either as part of a coating or as a complete matrix. Engineering pore distributions to match the mechanical properties of bone is commonly accepted to be the next major improvement in the design of open-cell porous materials. This means that a technique needs to be available that will allow the precise positioning of pores in the 3-D matrix, their inter-connectivity, shape and size. The use of adequate techniques of RP can provide the technological platform for this precise pore positioning [10].

RP developments mainly focused on polymer and ceramic materials. The transfer of RP technologies to metal materials for tissue engineering and orthopaedic implants possesses a significant challenge. There are few investigators on making metal scaffold for orthopaedic and tissue engineering application by rapid prototyping techniques. Two methods were applied to make metal scaffold, one is indirect to make porous scaffolds by invest casting melt metal or metal powder slurry into a mould where the mould was made using RP , in addition to indirect processing, other have been developing porous titanium scaffolds for tissue engineering using direct metal deposition. A key feature of this technology is the 3D computer-controlled fibre depositing of Ti6Al4V slurry at room temperature to produce a scaffold, consisting of layers of directionally aligned Ti6Al4V fibres. Porous Ti6Al4V scaffolds were successfully fabricated directly by a rapid prototyping technique, 3D fibre deposition. It is shown that Ti6Al4V slurry is a key point for building 3D scaffolds. Three main parameters of the fibre depositing process: the dispensing pressure, feeding speed and initial height between nozzle and platform were investigated for its effect on the integrity of scaffolds fabricated [11].

Rapid prototyping (RP) is a novel technique that allows the fabrication of porous materials with a well-defined structure and controlled porosity. The porous titanium scaffolds were prepared by using a rapid prototyping method.

The porous titanium scaffolds were evenly covered by a CaP coating using supersaturated solutions and electro deposition. The coating consisted in carbonated hydroxyapatite and presented good adhesive properties to the Ti substrate. RBMC seeded on the Ti scaffolds proliferated and colonized the entire porosity. After subcutaneous implantation, histology revealed the presence of mineralized collagen but not mature bone tissue. This study opens up the possibility of using high strength porous scaffolds with appropriate osteo conductive and oestrogenic properties to reconstruct large skeletal parts in the maxillofacial and orthopaedic fields [12].

2.2.3 Tissue engineering

Tissue engineering is a rapid developing new area of science and many exciting results have been published recently. The main focus of tissue engineering was on the culture of cells for the last ten

This project has been funded with support from the European Commission. This publication [communication] reflects the views only of the authors, and the Commission cannot be held responsible for any use which may be made of the information contained therein.

years. The generation of functional implants from living cells becomes now more and more important. Therefore, the three dimensional (3D) structure and its generation begins to play an essential role. In general, organs are 3D structures composed out of living cells and a support structure. According to their mechanical strengths the supports can be classified as soft and hard tissue. Scaffolds are of great importance for tissue engineering because they enable the production of functional living implants out of cells obtained from cell culture. These scaffolds require individual external shape and well defined internal structure with interconnected porosity. The problem of the fabrication of prototypes from computer assisted design (CAD) data is well known in automotive industry. Rapid prototyping (RP) techniques are able to produce such parts. Some RP techniques exist for hard tissue implants. Soft tissue scaffolds need a hydrogel material. No bio functional and cell compatible processing for hydrogels exists in the area of RP [13].

Direct fabrication of custom implants is promising in offering simpler and more rapid surgical implementations.

The potential to intimately control the microstructure of porous channels and the overall macroscopic shape of the implants makes RP an ideal process for fabricating implant and tissue engineering scaffold as well. There are also two particular characteristics of RP systems that limit their performance. One is the overall resolution of the processes achievable in current systems and the second is the ranging materials from which prototypes are made.

The use of a non resorbable bio ceramic composite system consisting of hydroxyapatite particles bonded together by a calcium phosphate glass phase to build a biocompatible bone for implant. The implant built is almost completely dense, which renders it unsuitable for use in its intended application in bone tissue engineering. Although this kind of process has an advantage in its ability of recreating the external shape of the scaffold, it unfortunately still suffers the limitation of a lack of microstructure control, because the microstructure of each sheet is uniform. By using 3DP to build drug delivery devices and tissue regeneration devices, only polyethylene oxide (PEO) and polycaprolactone (PCL) powders were used in the experiments, theoretically and virtually any materials that can be processed into powdered form can be used for 3D printing. In order to create TE scaffolds by RP techniques, it is desirable that the current materials be replaced by biomaterials that can satisfy the biocompatibility and biodegradability. Each RP process has its own advantages and disadvantages in building TE scaffolds. In terms of trapped material removal, FDM has a major advantage as no support material is needed during the fabrication of scaffolds. Conversely, LOM has a major problem in producing micro channels since sheet material is pre-processed before lamination. In terms of suitability of material, SLS and 3DP processes have more diversity, as both polymer and ceramic powders are formable on current systems. In addition, the property of materials such as molecular weight has to be kept almost constant even after processed by RP processes without heating or with low temperature heating, such as 3DP, stand a better chance by minimizing the heating effect on materials. SLS has a major advantage that no binder is needed in the process, compared with 3DP [14].

This project has been funded with support from the European Commission. This publication [communication] reflects the views only of the authors, and the Commission cannot be held responsible for any use which may be made of the information contained therein.

Most tissue engineering (TE) strategies for creating functional replacement tissues or organs rely on the application of temporary three-dimensional scaffolds to guide the proliferation and spread of seeded cells in vitro and in vivo. The characteristics of TE scaffolds are major concerns in the quest to fabricate ideal scaffolds. It is essential structural characteristics and the pre-requisites for fabrication techniques that can yield scaffolds that are capable of directing healthy and homogeneous tissue development. Emphasis is given to solid freeform (SFF), also known as rapid prototyping, technologies which are fast becoming the techniques of choice for scaffold fabrication with the potential to overcome the limitations of conventional manual-based fabrication techniques. Many conventional fabrication techniques exist for TE scaffold production; these techniques are manual-based processes with characteristics that may not be suitable for achieving customized production. Further to this, the imperfections in scaffolds fabricated using the techniques due to the poor flexibility and control offered by the techniques, limit the application of the scaffolds. Computer-controlled fabrication via SFF technology may hold the key for a generic solution in automating scaffold production that can cater for variations in the shapes and requirements of different tissues and organs and also size variations between different individuals [15].

Polyhydoxyalkanoates (PHA) are polyesters produced by microorganisms under unbalanced growth conditions.

They are generally biodegradable and thermoprocessable, making them attractive as biomaterials for applications in both conventional medical devices and tissue engineering. Over the past years, PHA, particularly poly 3-hydroxybutyrate (PHB), copolymers of 3-hydroxybutyrate and 3-hydroxyvalerate (PHBV), poly 4-hydroxybutyrate (P4HB), copolymers of 3-hydroxybutyrate and 3-hydroxyhexanoate (PHBHHx) and poly 3-hydroxyoctanoate (PHO) and its composites have been used to develop devices including sutures, repair devices, repair patches, slings, cardiovascular patches, orthopedic pins, adhesion barriers, stents, guided tissue repair/regeneration devices, articular cartilage repair devices, nerve guides, tendon repair devices, bone marrow scaffolds, and wound dressings. The changing PHA compositions also allow favourable mechanical properties, biocompatibility, and degradation times within desirable time frames under specific physiological conditions [16].

The manufacture of poly[(R)-3-hydroxybutyrate-co-(R)-3-hydroxyhexanoate] (or PHBHHx) scaffolds, by means of an additive manufacturing technique based on a computer-controlled wet-spinning system, was investigated. By optimizing the processing parameters, three-dimensional scaffolds with different internal architectures were fabricated, based on a layer-by-layer approach. The resulting scaffolds were characterized by scanning electron microscopy, which showed good control over the fibre alignment and a fully interconnected porous network, with porosity in the range 79–88%, fibre diameter 47–76 µm and pore size 123–789 µm. Moreover, the resulting fibres presented an internal porosity connected to the external fibre surface as a consequence of the phase-inversion process governing the solidification of the polymer solution [17].

Stereolithography fabrication methods can be used to accurately prepare tissue engineering scaffolds with designs that can be modelled, allowing optimisation of the properties of the structures.

This project has been funded with support from the European Commission. This publication [communication] reflects the views only of the authors, and the Commission cannot be held responsible for any use which may be made of the information contained therein.

By varying the composition of the macromers and the pore architecture, scaffolds with a large range of mechanical properties can be obtained.

Characterisation of the scaffolds by micro-computed tomography shows excellent reproduction of the designs. The mechanical properties are evaluated in compression, and show good agreement with finite element predictions. The mechanical properties of scaffolds can be controlled by the combination of material and scaffold pore architecture.

The presented technology and materials enable an accurate preparation of tissue engineering scaffolds with a large freedom of design, and properties ranging from rigid and strong to highly flexible and elastic [18].

Porous ceramics are utilized in a number of application sectors in order to mitigate several processing, environmental, biological, or structural issues. The microstructure is primarily responsible for these properties and is a result of a particular processing technique. Additive manufacturing techniques also offer benefits over other techniques, particularly for the creation of bio-scaffolds for tissue engineering. Through the use of 3D imaging technology and additive manufacturing, scaffolds can be designed and fabricated to fit a patient's needs. The unique capability of controlling the exact architecture of the porous structure is also beneficial in the creation of pre forms for ceramic–metal composite manufacturing [19].

2.2.4 Dentistry

As in many branches of medicine, rapid prototyping is also used in dentistry for a range of dental specialties, including oral and maxillofacial prosthodontics surgery, dental implantology as a surgical guide or physical model. The use of RP in dental branches has many other benefits of which only one of them is medical modelling construction; there are so many useful fields, in which RP can be helpful, i.e. mass production of patterns for casting purposes. In this way, time consuming and/or difficult parts in restoration making can be easily implemented even without human intervention. Common technologies used in dentistry are stereo lithography (SLA), inkjet-based system (3D printing - 3DP), selective laser sintering (SLS) and fused deposition modelling (FDM). The materials that can be used are fairly diverse but, wax, plastics, ceramics and metals are all utilized by several teams for dental purposes.

Computer-directed rapid prototyping techniques have been used for dental therapy including the fabrication of all-ceramic restorations and orthodontic tooth movement for several years. The application of these technologies to dental education is waiting to be exploited. The teaching cube for operative dentistry instruction described is one example of the potential use of a newly developed rapid prototyping system to train tomorrow’s clinicians. This was to introduce these technologies to dental educators and encourage innovative ways to take advantage of them [20].

Medical implants and biological models have three main characteristics: low volume, complex shape, and can be customized. These characteristics suit very well with Rapid Prototyping (RP) and

This project has been funded with support from the European Commission. This publication [communication] reflects the views only of the authors, and the Commission cannot be held responsible for any use which may be made of the information contained therein.

Rapid Manufacturing (RM) processes. RP/RM processes are fabricated part layer by layer until complete shape finished from 3D model .

Biocompatible materials, such as Titanium and Titanium alloy, Zirconium, Cobalt Chromium, PEEK, etc, are used for fabrication process. Reverse Engineering (RE) technology greatly affects RP/RM processes. RE is used to capture or scan image of the limb, cranium, tooth, and other biological objects. Three common methods to get the image are 3D laser scanning, Computer Tomography (CT), and Magnetic Resonance Imaging (MRI). Main RP/RM techniques used in Dentistry are Stereotype Lithography Apparatus (SLA), Fused Deposition Modelling (FDM), Selective Laser Sintering (SLS), and ink jet printing. [21].

RP technologies have been employed for making medical prototypes in medicine and dentistry. Common technologies used in dentistry are stereo lithography (SLA), inkjet-based system (3D printing – 3DP), selective laser sintering (SLS) and fused deposition modelling (FDM). The materials that can be used are fairly diverse but, wax, plastics, ceramics and metals are all utilized by several teams for dental purposes. Just as RP, the aim of MRP (Medical Rapid Prototyping) is to fabricate dimensionally accurate physical models of human anatomy derived from medical image data using a variety of RP technologies. As in many branches of medicine, this term has been also used in dentistry for a range of dental specialties, including oral and maxillofacial prosthodontics and surgery. The use of RP in dental branches has many other benefits of which only one of them is medical modelling construction; there are so many useful fields, in which RP can be helpful, i.e. mass production of patterns for casting purposes. In this way, time consuming and/or difficult parts in restoration making can be easily implemented even without human intervention [22].

Stereo lithography is now applied quite generally for diverse applications, in biomedical engineering there is a particularity, which is in the use of the scanner (X tomography). In these well-known techniques, especially for practitioners, the object (bone, skull...) is sliced physically. It was natural to do the parallel with stereo lithography and to transfer the slices of scanner to the slices of the stereo lithography and then to have quite in real time a copy in 3-D (with all the inside) of the skull, bones, and so on [23].

RP techniques have been substantially employed in medicine; however, the applications of RP in dental area are relatively rare. Every RP technique starts with a CAD model. The construction of a CAD model and its associated techniques, including the data scanning modalities, data acquisition, data processing, and use of CAD packages.

Both general purpose and specific software packages commercially available greatly benefit the design of CAD models. With the help of various RP techniques, the fabrication of dental objects can be done easily and rapidly. It is difficult to generate them by NC machining because of features like overhangs, sharp corners, and undercuts in most dental objects. The diversity of RP systems and corresponding build materials makes it possible to generate dental objects with different needs (colour, transparency, and material) for different applications like custom implant design. It is clear that the use of RP models in dental application will be expanded in the future with the ongoing

This project has been funded with support from the European Commission. This publication [communication] reflects the views only of the authors, and the Commission cannot be held responsible for any use which may be made of the information contained therein.

development of RP techniques. A number of application examples were studied, which demonstrate that RP techniques are playing a more and more important role in dental application. RP models will benefit dentistry in many areas including surgical planning, prosthesis design, and so on [24].

The method of making titanium dental crowns by means of integrating laser measuring, numerical simulation and rapid prototype (RP) manufacture of wax patterns for the investment casting process have been studied. In this process, four real tooth crowns were measured by means of 3D laser scanning. The laser digitized geometry of the crowns was processed and converted into standard CAD models in STL format, which is used by RP systems and numerical simulation software. Commercial software (MAGMASOFT) was used to simulate the casting process and optimize the runner and gating system (sprue) design. RP crowns were `printed' directly on a Model Maker II 3D Plotting System. A silicone negative mould (soft tool) was made from the RP crowns, and then more than hundreds wax crowns was duplicated. The duplicated crowns were joined to the optimized runner and gating system. By using the investment casting process 20±25 replicas of each crown were made on a centrifugal casting machine. All castings were examined for porosity by X-ray radiographs. By using the integrated scanning, simulation, RP pattern and casting procedure, cast crowns, free of porosity, with excellent functional contour and a smooth surface finish, were obtained from the first casting trial. The coupling of laser digitizing and RP indicates a potential to replace the traditional impression taking and waxing procedure in dental laboratory, with the quality of the cast titanium prostheses also being improved by using the numerically optimized runner and gating system design [25].

The first digital revolution took place with the production of dental restorations such as veneers, inlays, crowns and bridges using dental CAD–CAM systems and new improved systems appear on the market with great rapidity.

The reducing cost of processing power will ensure that these developments will continue as exemplified by the recent introduction of a new range of digital intra-oral scanners. With regard to the manufacture of prostheses is currently dominated by subtractive machining technology but it is inevitable that the additive processing routes of layered fabrication, such as FDM, SLA, SLM and inkjet printing, will start to have an impact. In principle there is no reason why the technology cannot be extended to all aspects of production of dental prostheses and include customized implants, full denture construction and orthodontic appliances. In fact anything that might expect a dental laboratory to produce can be done digitally and potentially more consistently, quicker and at a reduced cost.

Dental device manufacturing will experience a second revolution when layered fabrication techniques reach the point of being able to produce high quality dental prostheses. This can potentially take dental materials research in a totally different direction [26].

This is to determine the dimensional accuracy of the skull models produced using the rapid prototyping technology of stereo lithography apparatus with the aim of validating the system for clinical applications. The data for this validation study was derived from 3D computed tomography (CT) images of dried human adult skulls and replica models of those images were produced for analysis.

This project has been funded with support from the European Commission. This publication [communication] reflects the views only of the authors, and the Commission cannot be held responsible for any use which may be made of the information contained therein.

The resultant 2-D images were stored in Digital Imaging and Communications in Medicine (DICOM) format. The segmentation of the images was prepared in MIMICS software. The slice files were then exported to a stereo lithography apparatus (SLA) to produce the replica of each skull. Eight linear measurements were repeatedly made between identified landmarks on each of the original skull and its replica model using an electronic digital calliper. The study showed that the accuracy of the replica models produced by the stereo lithography apparatus is appropriate within a margin of error that is acceptable for clinical applications in dental and craniofacial surgery [27].

The material used for fabricating dentures should have good mechanical and tribological properties in order to withstand heavy forces inside the mouth. A study has been made to evaluate the hardness and tribological properties the Poly (Methyl methacrylate) PMMA based denture composite reinforced with seashell nano powder. The PMMA bio composites containing 2%, 4%, 6%, 8%, 12%, 16% and 20% by weight of seashell nano powder and an unfilled composite as control specimen were fabricated. The micro hardness of the composites was found using Vickers hardness tester. The addition of 2% seashell nano powder had no significant effect on the micro hardness. But it was found that on increasing the seashell nano powder content, the micro hardness value increased till 12% and substantially decreased beyond 12% seashell nano powder. The wear test was performed and frictional forces generated during sliding of specimens were evaluated in pin on disc apparatus. The wear mechanism and dispersion of seashell nano powder in the specimen were analyzed in Scanning Electron Microscopy (SEM). The wear resistant property increased on addition of seashell nano powder with 12% seashell nano powder reinforced composite showing least frictional force developed during the wear test. The 16% and 20% filled composite developed more frictional force than developed in 12% filled composite. It was concluded that PMMA bio composite could be successfully reinforced by seashell nano powder with better properties at 12% seashell nano powder content followed by 8% filled composite [28..

In tab. 1 examples of materials, technologies and applications of models imitating soft tissues was presented.

Table 1. Materials, technologies and applications of models imitating soft tissues [29]

S.no	Authors	Year	Dyscypline	Materials	Technology
1	R. A. Watson	2014	Hepatology	- Nylon	- Selective Laser Sintering
2	Y. Zheng et al.	2016	Hepatology	- ABS	- Objet 500 Connex 3 (Polyjet)

This project has been funded with support from the European Commission. This publication [communication] reflects the views only of the authors, and the Commission cannot be held responsible for any use which may be made of the information contained therein.

3	J. S. Witkowski et al.	2017	Hepatology	- PLA - Silicone rubber – Polastosil M-2000	- Ultimaker 2+ (FFF) cast + internal structures - Manual casting
4	A.M. Blanco et al.	2018	Hepatology	- PLA Shenzhen Esun Industrial Co. / Colorfila - PVA Shenzhen Esun Industrial Co. – support material - Silicone rubbers: a) The Smooth-On EcoFlex 00-30 b) SortaCLEAR Shore A 18 c) ClearFlex 30 by SmoothOn	- Sigma BCN3D (FFF) – cast + internal structures - Manual casting (material a)) - Renishaw Vacuum System 5/01(material b)) - Manual casting (material c))
5	C. L. Cheung et al. [M3]	2014	Urology	- Powder ZP-131 + bonding agent ZB-60 - Infiltration process Z-Bond 90 - Silicon rubber – Dragon Skin 30 + Slacker Tactire Mutator (SmothOn)	- Spectrum Z510 3D Printer (Inkjet Printing) - cast - Manual casting + vacuum chamber (degassed process)
6	JC. Bernhard et al.	2015	Urology	- Photopolymer	- Objet 500 Connex 3 (Polyjet)
7	F. Adams et al.	2016	Urology	- Engineered wax material - Photopolymer VeroClear - Silicone rubber – The SmoothOn Ecoflex 00-20 - Agarose gel – Agarose Electran - Polydimethylsiloxane (PDMS)	- 3Z Pro, Solidscape (high precision 3d printing) – inner wax mold - Objet 260 Connex 3 (Polyjet) – external cast - Manual casting
8	H. Lee et al.	2018	Urology	- Photopolymer	- Objet 260 Connex 3 (Polyjet)
9	H. Riedle et al.	2020	Cardiology	- ACEO® Silicone GP Shore A 20	- ACEO® Technology (drop-on-demand 3D printing)

This project has been funded with support from the European Commission. This publication [communication] reflects the views only of the authors, and the Commission cannot be held responsible for any use which may be made of the information contained therein.

10	S. R. de Galarreta	2013	Cardiology	- Full-cure 720 - Silicone rubber – SLM VTX 950 - WA-70 wax - Resin – SLM PUR	- Objet Eden 330 (Polyjet) – master model - Manual casting - MCP 4/01 Vacuum Casting Machine
11	I. O. Torres et al.	2017	Cardiology	- Polyjet Material Rubber FLX930 - Polyjet Material Standard Plastic RGD810 - Polyjet Digital Material Tango Plus + Vero Clear Shoe 60 - Flexible Photopolymer Resin for Form1+ - MakerBot Tough PLA	- Objet 350 Connex 3 (Polyjet) - Formlabs Form1+ (SLA) - Makerbot (FFF)
12	T. Mashiko et al.	2015	Neurology	- ABS - M8012 fromAsahi Kasei-Wacker Silicone (molding silicone)	- UP!Plus 3D Printer (FFF) - Manual coating
13	J. R Ryan et al.	2015	Neurology	- Gypsum powder - ABS - Casting silicone - The Smooth-On Mold-Max 60 - Hydrogel (gelatin + agar gel powder)	- zPrinter 350 (Inkjet Printing) - Stratasys Dimension 1200es (FFF) - Manual casting
14	J.P. Thawani et al [M15]	2016	Neurology	- Polycarbonate-like photoreactive polymer	- ProJet 6000 3D Printer (SLA)
15	J. R. Ryan et al.	2016	Neurology	- Photopolymer Shore A 27 - ABS - Silicone rubber – The SmoothOn Mold Star	- Objet 500 Connex 3 (Polyjet) - Stratasys Dimension 1200 (FFF)

This project has been funded with support from the European Commission. This publication [communication] reflects the views only of the authors, and the Commission cannot be held responsible for any use which may be made of the information contained therein.

				- Silicone Rubber – DragonSkin + Slacker Tactire Mutator (The SmothOn) - Composite Material	- zPrinter 650 (Inkjet Printing)
16	W. Mussi et al.	2020	Neurology	- PLA - PLA wood-loaded - Silicone rubber – The SmoothOn EcoFlex 00-50 - Silicone rubber – DragonSkin 10	- MakerBot Replicator 2X (FFF) - Manual casting
17	S.Bustamante et al.	2014	Pulmonology	- Photosensitive flexible liquid resin	- Object 350 Connex3 (Polyjet)
18	S.N. Kurenov et al. [M12]	2015	Pulmonology	- TangoPlus (Thermoplastic elastomer)	- PolyJet Eden 260 V (Polyjet) - Objet 500 Connex 3 (Polyjet)
19	J. T. Lichtenstein et al.	2016	Ophthalmology	- PA2200 - Silicone mixture - VTV 800 (SLM Solution) + VTN 4500 (The SmoothOn)	- Selective Laser Sintering (bone + molds) - Manual casting
20	T. Byrne et al.	2016	Orthopedics	- Rubber-like material - Platinum-cure silicone gel - Ecoflex 00- 50; Smooth-On - High-detail polyamide - Highly concentrated gelatin solution	- Zcorp 3D printer (Inkjet Printing) - Manual casting

This project has been funded with support from the European Commission. This publication [communication] reflects the views only of the authors, and the Commission cannot be held responsible for any use which may be made of the information contained therein.

3 Mechanical testing of 3D printed parts – methods and standards

3.1. Hardness

Hardness is the measure of a material's resistance to local plastic deformation, formed on a small surface of the tested object, as a result of mechanical pressing into it of a second, harder body called the indenter, with a specific geometry. According to [30] the hardness of additively manufactured parts is measured using five methods: ball indentation method (plastics [31]), Vickers test (metals [32], ceramics [33]), Rockwell test (plastics [34]), Knoop test (ceramics [33]) and Shore test (plastics [35]).

3.1.1 Ball indentation method

This method involves the application of indenter in form of polished steel ball with the diameter of 5 mm. The test is carried out on hardness measuring instruments with an adjustable table and a fitted plate on which the test specimens are placed, an indenter with appropriate connectors and a system ensuring a non-impact load application. The device should be equipped with a sensor for measuring the imprint depth at a depth of 0.4 mm. Universal devices are often used, allowing for tests to be carried out using various methods (Fig. 3.1). Each test specimen should be a flat plate or block of sufficient parallelism between the test surface and the support surface. It is recommended to use specimens with a thickness of at least 4 mm, but it is essential that the surface to be supported does not exhibit any deformation after the test.

Fig 3.1 Universal hardness testing machine

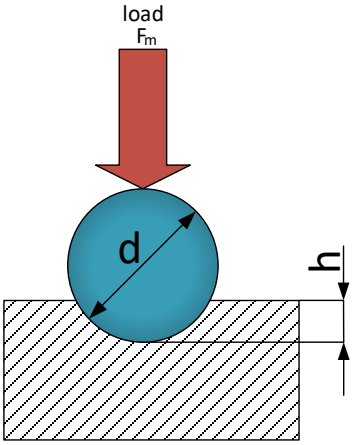

Fig 3.2 Scheme of hardness measurement by the ball indentation method

In order to carry out the test, the test sample is placed on a supporting plate so that the shaped piece rests completely on it and the test surface is perpendicular to the direction of load application.

This project has been funded with support from the European Commission. This publication [communication] reflects the views only of the authors, and the Commission cannot be held responsible for any use which may be made of the information contained therein.

Then a preload of 9.8 N is applied at a distance not less than 10 mm from the edge of the specimen, and then smoothly apply the load F_m, which should be one of the four values: 49 N, 132 N , 358 N or 961 N. They shall be chosen in such a way that, after a thirty-second loading, the depth of the resulting impression h will have value between 0.15 mm and 0.35 mm. The test should be carried out at least ten times and the final result should be the arithmetic mean of all measurements. The hardness measured by the ball indentation method is defined as the ratio of the pressing force to the surface of the resulting impression, however, it is necessary to take into account a number of corrections for disturbances caused by, among others, deformation of the device frame. Resulting formula for hardness calculation takes the form:

$$HB = \frac{F_m \frac{0{,}21}{h - 0{,}25 + 0{,}21}}{\pi\, d\, (h - 0{,}25)} \tag{3.1}$$

3.1.2. Vickers test

To measure the hardness by the Vickers method, the diamond indenter in the shape of a regular pyramid with an apex angle equal to $\alpha = 136°$ is used (Fig. 3.3).

After the indenter is brought into contact with the test sample, it should be loaded with nominal force of 294 N (other load values are allowed) without shocks and vibrations. The time from the beginning of load application to reaching the nominal load should be from 2 to 8 seconds, while the standard loading time from 10 to 15 seconds.

Specimens of any shape can be used, but the test surface must be perpendicular to the direction of the indenter's action. In addition, at the measurement site, the sample should be free from contamination and polished so that machining traces do not affect the accuracy of the measurement.

The Vickers hardness is the ratio of the load F to the lateral surface area of the impression S, taking into account the necessity to convert the force expressed in kilograms of force into newtons:

$$HV = 0{,}102\frac{F}{S} = 0{,}102\frac{F}{\frac{d^2}{2\sin\left(\frac{\alpha}{2}\right)}} \approx 1{,}891\frac{F}{d^2}$$

where $d = \frac{d_1+d_2}{2}$ is mean length of indentation diagonal (Fig. 3.4). For the result shall be the arithmetic mean of three consecutive measurements. The anisotropy of the material, typical of additive manufacturing parts, can result in a distorted imprint. Calculation of the Vickers hardness value, when the prints have concave or convex sides (Fig. 3.4), requires taking into account the so-called O'Neil's corrections, leading to a modified expression:

This project has been funded with support from the European Commission. This publication [communication] reflects the views only of the authors, and the Commission cannot be held responsible for any use which may be made of the information contained therein.

$$HV \approx 1{,}891 \frac{F}{\left(\frac{d + b\sqrt{2}}{2}\right)^2}$$

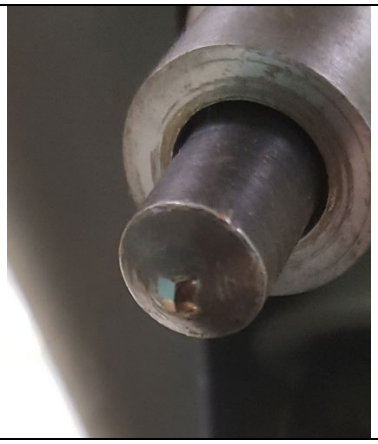

Fig. 3.3 Vickers test intender

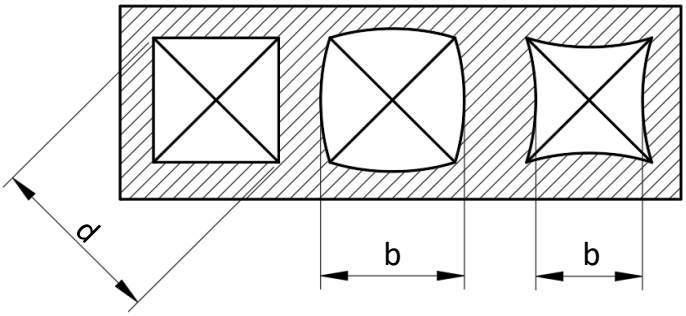

Fig. 3.4 Vickers test imprints

In order to reduce the influence of measurement errors on the results, it should be performed at least three times and the arithmetic mean of all measurements should be taken as the result.

3.1.3. Rockwell test

A characteristic feature of the Rockwell hardness test is the two-stage load application to the indenter. During the first step, a minor load of 100 N is applied. Then, in ten consecutive seconds, the load is increased to main (major) value, held for a further 15 seconds, and then released, sustaining only the minor load. The difference in depth e of the impression is measured before and after the application of the major load (Fig. 3.5). The Rockwell hardness is expressed numerically by substituting the measured difference of depression e into the following expression:

$$HRx = 130 - \frac{e}{0.002}$$

where x denotes measurement scale. The test specimen should be a plate with a minimum thickness of 6 mm and a surface allowing five measurements to be made on it, in such a way that the distance between the two measurement points is not lesser than 10 mm. When testing the hardness of an anisotropic material, the samples should be prepared in such a way that five measurements can be made for each direction.

This project has been funded with support from the European Commission. This publication [communication] reflects the views only of the authors, and the Commission cannot be held responsible for any use which may be made of the information contained therein.

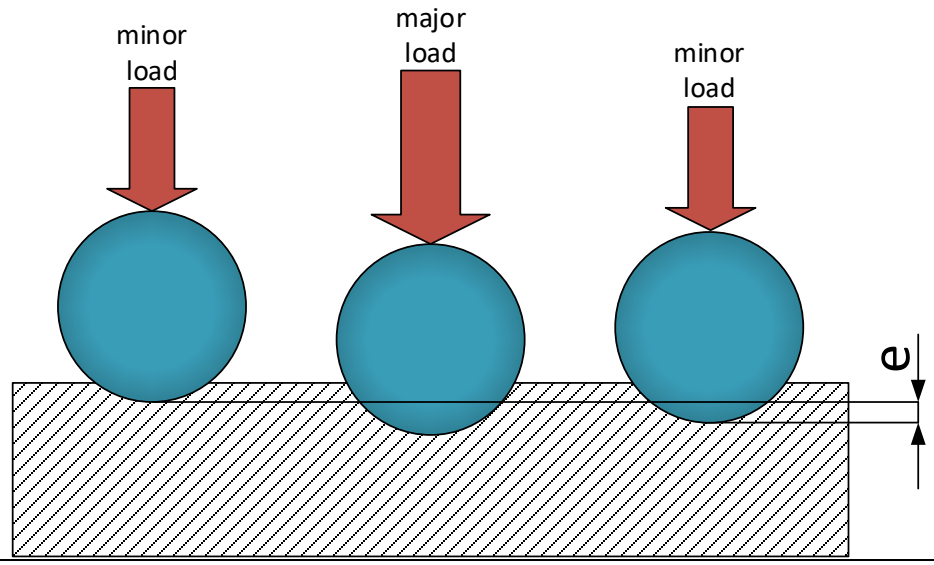

Fig. 3.5 Rockwell test scheme

The value of the major load and the type of indenter used depend on the scale on which the test is carried out. According to [33], the Rockwell hardness of plastics is tested on the scales L, M and R, the features of which are presented in Table 3.1.

Table 3.1. Characteristics of Rockwell scales for testing the hardness of plastics

Scale	Intender	Major load
L	*1 Ø 6.35 mm Steel ball*	60 N
M	*2 Ø 6.35 mm Steel ball*	100 N
R	*3 Ø 12.70 mm Steel ball*	60 N

3.1.4. Shore test

Two different methods of hardness measurement can be called the Shore test. One of them is the dynamic method of measuring the hardness of metal materials, while the other, also called durometer test, is utilized to test the hardness of non-metal materials [6] and it is used in the context of additive manufactured parts.

This project has been funded with support from the European Commission. This publication [communication] reflects the views only of the authors, and the Commission cannot be held responsible for any use which may be made of the information contained therein.

Determination of hardness by means of a Shore durometer consists in measuring the resistance of a sample of the tested material during the penetration of an indenter needle with a specific shape and size, placed in the base of the measuring instrument. The minimum thickness of the test specimen should be 4 mm, layering of specimens to obtain the minimum thickness is allowed. The sample must allow for the measurement to be made at least 9 mm from the edge and have flat surfaces with a minimum radius of 6 mm. As a standard, a minimum of five measurements are made at different locations on the sample, at least 6 mm apart, and the mean value is calculated.

The test is carried out in one of two scales - A or D, which are determined by the type of indenter used (Fig. 3.6 a, b). The A type indenter is used for soft materials, while the D type is for hard materials. The Shore hardness is denoted as $Shx\ N$, where x is the method and N is the value read from the durometer. The advantage of the method is the pocket size of the measuring apparatus (Fig. 3.7), allowing measurements to be carried out on a functional part without the need to disassemble it.

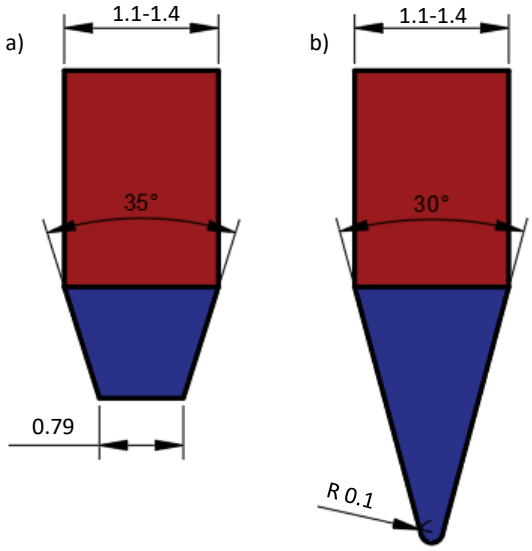

Fig. 3.6 Shore durometer's intenders: a) type A, b) type D

Fig. 3.7 Shore duroemeter [36]

3.1.5. Knoop test

The method was developed as an alternative to the Vickers method, from which it differs with the indenter used. Here it takes the form of a diamond pyramid with a diamond base. The opposite edges of the solid angle of the pyramid form different angles, with the major angle of 172,5° and the minor angle of 130°. The imprint projection is always a rhombus, the diagonal lengths of which are always equal to d and $7d$. The indenter designed in this way allows to make repeatable imprints of even small pressing forces $F = 10 \div 20N$. This method is therefore used to test the hardness of materials in which making a deep imprint is undesirable, e.g. due to the risk of breakage in the case of ceramics. The Knoop hardness value is determined from the formula:

This project has been funded with support from the European Commission. This publication [communication] reflects the views only of the authors, and the Commission cannot be held responsible for any use which may be made of the information contained therein.

$$HK = 14.228\frac{0.102F}{(7d)^2}$$

3.2. Tensile strength

Tensile strength is the maximum tensile stress, considered as the tensile force related to the initial cross-sectional area that can be induced in the material. This parameter is determined during the static tensile test, which is the basic and most common method of testing materials.

The test consists in stretching the normalized sample axially at a constant speed until the failure. The test is carried out using universal testing machines (Fig. 3.8). During the test, the dependence of the tensile force on the sample length increment is recorded. The finished plot resulting from this measurement is presented as nominal stress versus nominal strain.

Sample graphs from the static tensile test are shown in figure 3.9. In elasto-plastic materials (Fig. 3.9-a), after exceeding the tensile strength, there is a concentration of stress in the sample and its local narrowing occurs(formation of a neck), which is represented in the diagram by a decrease in stresses. In addition to the tensile strength, the graph can be used to read the longitudinal modulus (Young's modulus), yield stress, which is the limit stress at which permanent deformations occur in the sample, and strain at fracture. It should be noted that incrementally manufactured parts often do not retain this characteristic. Due to the materials used and the technology itself, the manufactured structure may not show a linear elastic area or a clear yield point (Fig. 3.9-b). Reaching the tensile strength is not always accompanied by the formation of a neck in the sample - rupture can occur suddenly. Moreover, brittle materials, such as sintered ceramics, do not undergo plastic deformation and often fail in the linear range (Fig. 3.8-c).

Fig. 3.8 Tensile machine

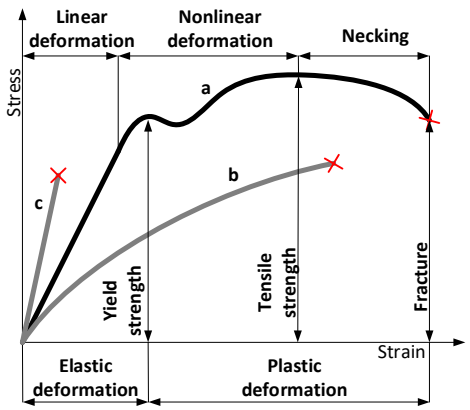

Fig 3.9 Static tensile test diagram

The static tensile test uses samples that differ in structure and dimensions. Most of them are clearly divided into the gripping part and the gage (Fig. 3.10). The cross-sectional area of the gage is usually smaller in relation to the grip part, so that the narrowing and breaking of the sample occurs

This project has been funded with support from the European Commission. This publication [communication] reflects the views only of the authors, and the Commission cannot be held responsible for any use which may be made of the information contained therein.

precisely in it. In order that deformations of the gripping part, resulting from the clamping of the tear-off jaws, do not disturb the uniaxial stress state in the working part, it is necessary to meet the appropriate dimensions of the specimen. These conditions are specified in the following standards: [37] (metals), [38] (plastics) and [39] (ceramics).

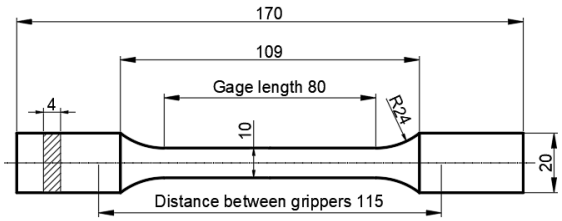

Fig 3.10 Typical specimen for testing the tensile strength of plastic material

There are also many ways to grasp the sample, which obviously affects the geometry of the grip part. The most commonly used ends of a round (Fig. 3.11-b) and a flat (Fig. 3.11-e) sample are often embedded in self-tightening collars for a secure grip. The standards also allow the use of other ends that provide positive engagement with the machine chuck, including threaded (Fig. 3.11-a), blunt (Fig. 3.11-c) and pin (Fig. 3.11-d) ends. The proper choice of the gripper structure is to prevent the sample from slipping out of the jaws and to minimize the bending moments.

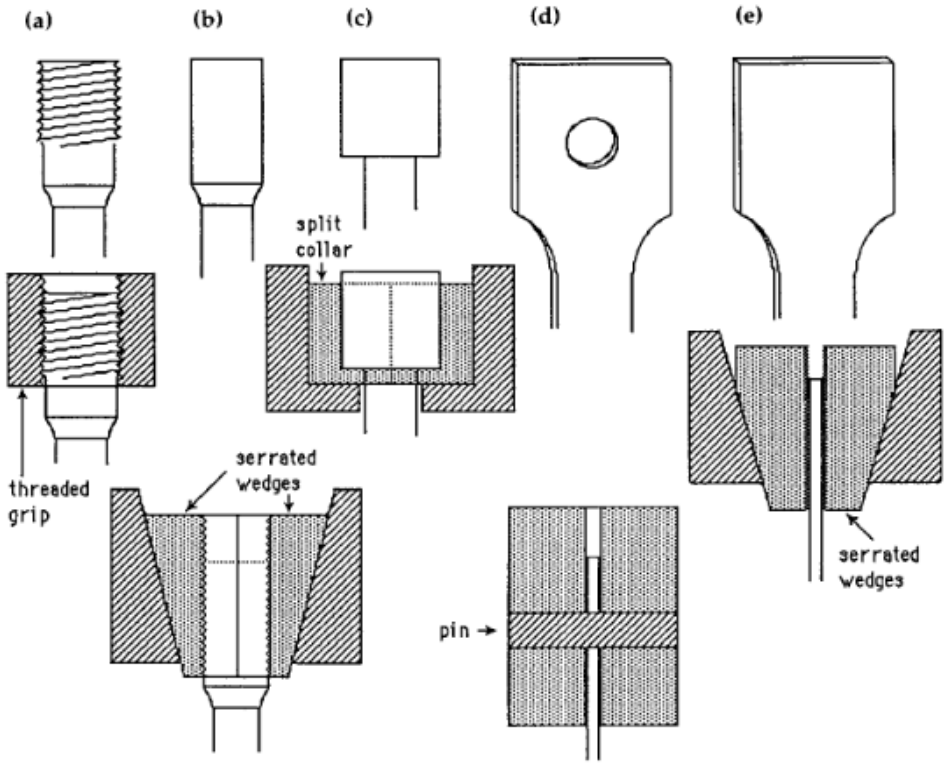

Fig. 3.11 Different types of griping ends of tensile test specimens [40]

This project has been funded with support from the European Commission. This publication [communication] reflects the views only of the authors, and the Commission cannot be held responsible for any use which may be made of the information contained therein.

3.3. Impact strength

Impact strength is the resistance of a material to cracking under dynamic loading. Impact strength is defined as the ratio of the work required to break a standardized specimen to the cross-sectional area of the specimen. Standard [30] indicates two methods of measuring the impact strength of additively manufactured samples: the Charpy method [41, 42, 43] and the Izod method [44].

3.3.1 Charpy test

The test consists in breaking with one blow of a falling pendulum hammer the specimen supported at both ends with a rectangular cross-section with a notch in the middle of its length. The sample should lie in such a way that the blade of the pendulum knife hits it on the opposite side of the notch.

The test is carried out on a device called a Charpy hammer (Fig. 3.12). It allows for the determination of the energy required for the impact fracture of the sample supported with its ends on two supports by means of a pendulum hitting it in the center. The breaking work is the difference of the hammer potential energy in the initial and final position, which is easy to calculate knowing the hammer mass moment of inertia and initial and final angular orientation of the pendulum (Fig. 3.13).

Fig 3.12 Charpy hammer

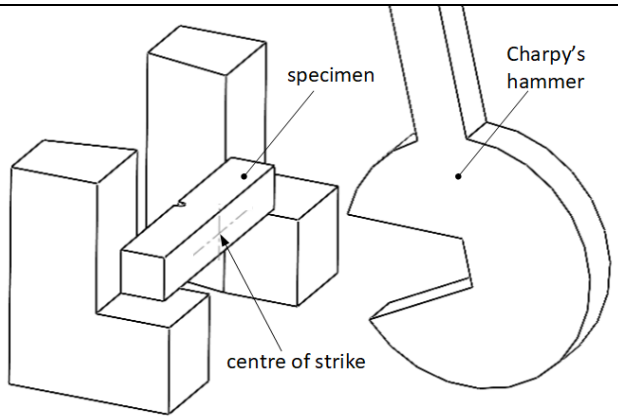

Fig 3.13 Method of embedding the sample in the measuring device

Two types of samples are used in the Charpy test - U (Fig. 3.14) and V (Fig. 3.15). Based on [41] and [42], Table 3.2 shows the dimensions of these samples.

This project has been funded with support from the European Commission. This publication [communication] reflects the views only of the authors, and the Commission cannot be held responsible for any use which may be made of the information contained therein.

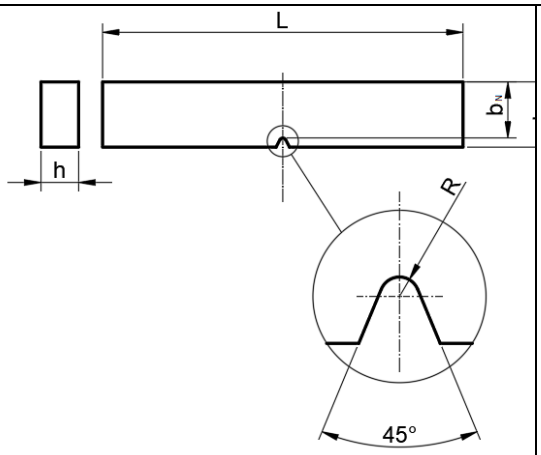

Fig 3.14 Test specimen with V-notch

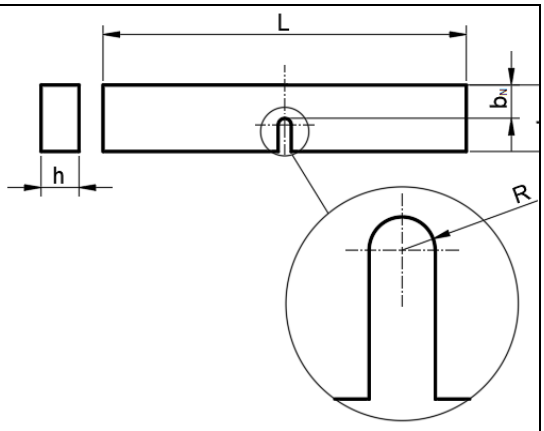

Fig 3.15 Test specimen with U-notch

Table 3.2 Specimens dimensions for Charpy test

Material	Specimen type	Length L	Width h	Height b	Height under the notch b_N	Notch radius R
Metal	U	55	10	10	8	1
	V	55	10	10	8	0,1
						0,5
						1
Plastic	U	80	10	4	8	1

3.3.2 Izod test

The essence of the Izod impact test is similar to that carried out by the Charpy method, but in this case only one side of the sample is fixed - the other side remains free (Fig. 3.16). For this test, V-notch or un-notched samples are used, the dimensions of which are indicated in Table 3.3.

This project has been funded with support from the European Commission. This publication [communication] reflects the views only of the authors, and the Commission cannot be held responsible for any use which may be made of the information contained therein.

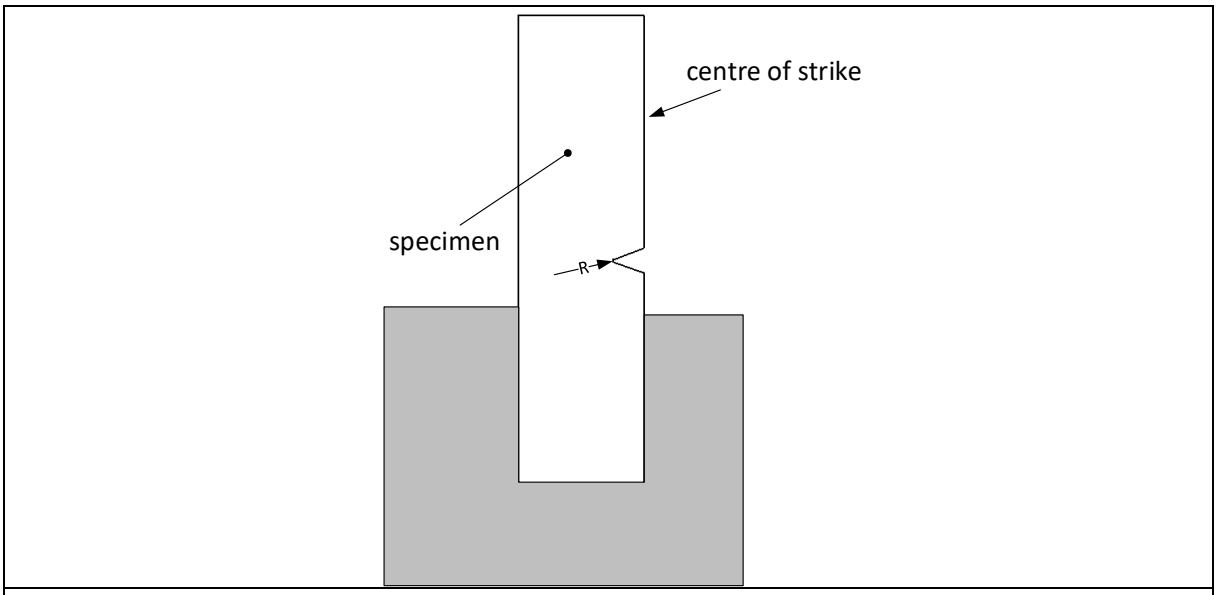

Fig 3.16 Embedded sample during the Izod test

Table 3.3 Specimens dimensions for Izod test

Specimen type	Dimensions $L \times b \times h$	Notch type	Notch radius R	Height under the notch b_N
U	80x10x4	Without notch	-	8,0
A		A	0,25	
B		B	1	

3.4. Compressive strength

Compressive strength is defined as the maximum stress that can be withstand by the specimen under the compression loads. The compressive strength of a material is determined by a test called static compression test. It consists in compressing a sample between two flat plates with a force of a known value and recording the deformation caused by this force.

This project has been funded with support from the European Commission. This publication [communication] reflects the views only of the authors, and the Commission cannot be held responsible for any use which may be made of the information contained therein.

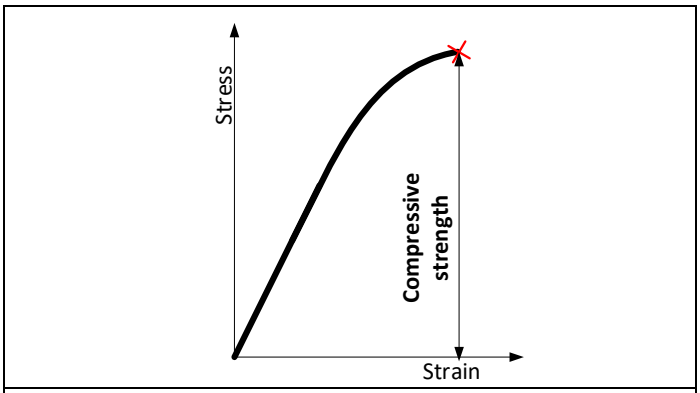

Fig. 3.17 Static compression test diagram

Seemingly, the compressive strength test differs from the tensile strength test only in the direction of the force applied, but in reality the test is much more difficult to carry out. Compression will be accompanied by an increase in the transverse dimension of the sample, but the friction between the sample and the clamping plates limits the free slide, thus leading to a triaxial stress state in the sample. The solution may be to use sufficiently long samples, but this may cause the sample to buckle during the test. For this reason, it is particularly important to use samples for normative tests.

The dimensions of plastic samples and the test procedure are regulated by [45]. According to it, the samples may have the shape of a cuboid, cylinder or tube with a length of 50 (for the module test) or 10 (for the compression strength test) millimeters and width or outer diameter of 10 mm. If it is not possible to use a specimen with the dimensions indicated, the more general rule is applied to describe the relationship between the specimen length l and the specimen diameter or side length x and the maximum specimen strain ε_c^*:

$$\varepsilon_c^* \leq 0{,}4\frac{x^2}{l^2}$$

The International Organization for Standardization does not specify a standard for testing the compressive strength of metals. On the basis of the [46] standard, however, recommendations can be made as to the size of the samples for this test - it is expected to use three types of cylindrical samples differing in slenderness. Their dimensions are presented in table 3.4. For testing very brittle materials, such as ceramics, it is suggested to use specimens in form of dog-bones [47].

Table 3.4 Dimension of metal specimens for static compression test

Specimens	Diamenter	Length	Length/Diameter ratio
Short	30	25	0.8
	13	25	2.0
Medium	13	38	3.0
	20	60	3.0

This project has been funded with support from the European Commission. This publication [communication] reflects the views only of the authors, and the Commission cannot be held responsible for any use which may be made of the information contained therein.

	25	75	3.0
	30	85	3.0
Long	20	160	8.0
	30	320	10.0

3.5. Flexural strength

The flexural strength is the contractual stress corresponding to the highest loading force obtained during the bending test. When these stresses are exceeded, the material is destroyed. The bending strength test is carried out by three-point or four-point bending with a constant speed of a prismatic sample on devices called benders.

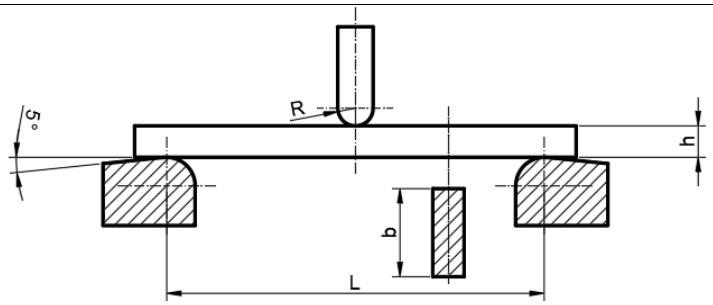

Fig. 3.18 Flexural strength test bench

The bender should be equipped with two supports with adjustable distance L, allowing for easy mounting of the tested specimen on them, and a pressing pin with a suitable rounding radius R exerting pressure on the sample at exactly half the distance between the supports (Fig. 3.18). Before starting the test, the clamp should be brought into contact with the specimen in such a way that it will be not preloaded. During further loading of the clamp, the values of the clamping force and the corresponding deflection arrows are recorded until the break of the specimen.

The shape and dimensions of specimens for bending strength tests differ depending on the type of tested material. Guidance on specimen dimensions and the measurement procedure for metals is included in [48]. For testing plastics, it is recommended to have rectangular samples with dimensions of 80x10x4, but the standard [49] also allows the use of other samples, as long as they meet the criterion:

$$\frac{L}{h} \approx 20$$

while maintaining an appropriate relationship between the thickness h and the width b (Table 3.5).

Table 3.5 Dimensions of the specimen for the flexural strength test of plastics

Thickness h	Width b
$1 < h \leq 3$	25
$3 < h \leq 5$	10
$5 < h \leq 10$	15
$10 < h \leq 20$	20
$20 < h \leq 35$	35
$35 < h \leq 50$	50

This project has been funded with support from the European Commission. This publication [communication] reflects the views only of the authors, and the Commission cannot be held responsible for any use which may be made of the information contained therein.

Specimens for testing ceramic materials should have a rectangular (type A and type B) or round (type C) cross-section. Their dimensions are shown in Table 3.6 [50].

Table 3.6 Dimensions of the specimen for the flexural strength test of ceramics

Type	Length	Width/diameter	Height
A	35	5	5
B	20	6.5	5.25
C	25	3.3	-

3.6. Fatigue strength

Material fatigue is defined as change occurring in the material under the influence of periodically changing stresses, which can lead to the destruction of the material. A characteristic feature of the fatigue failure of the material is that it occurs at stresses much lower than the ultimate strength, and even the yield strength. Fatigue cracks have the character of brittle cracks. They are particularly dangerous because the formation of the fatigue crack often goes unnoticed, and the final failure of the parts occurs suddenly and unexpectedly, usually leading to dangerous failures.

The fatigue resistance of parts depends on the type and properties of the material, the shape of the element, the range of stress variability in the material, the type of surface treatment and the smoothness of the surface. Considering the last two factors, it should be concluded that additive manufactured parts are particularly vulnerable to this type of failure.

The fatigue strength tests are clearly divided into tests of material samples, taking into account the method of surface treatment and smoothness, as well as shape fatigue strength tests, i.e. testing of finished technical elements with complex shapes. The group also includes tests of samples with various types of notches made on them, aimed at determining the effect of stress concentration in the notches on the reduction of fatigue strength. Sometimes whole construction teams and even finished devices are subjected to special fatigue tests.

The classic method of testing the fatigue strength consists in drawing up the Wöhler diagram. The minimum number of samples needed for this purpose is 8 pieces. The first sample is loaded so that the maximum stress is about 66% of the tensile strength. After the first specimen fails, the load on the second and subsequent specimens is selected in such a way as to obtain successively lower maximum stresses, while the same mean stress. By reducing the stress, an increasing number of cycles are obtained at which the specimens break. The measurement points of the relationship between the maximum stress and the number of cycles that the specimens will withstand are arranged near certain curve called the Wöhler curve (Fig. 3.19). For some materials, including steel, the Wöhler curve has a horizontal asymptote greater than zero, which means that there are limit stresses for them below which the sample will not fail under any number of load cycles (Fig. 3.19-a). These stresses are called unlimited fatigue strength. For other materials and most additively manufactured parts, unlimited

This project has been funded with support from the European Commission. This publication [communication] reflects the views only of the authors, and the Commission cannot be held responsible for any use which may be made of the information contained therein.

fatigue strength does not exist - the limited fatigue strength is then defined as the maximum stress at which the material (part) will not fail within a certain number of cycles (Fig. 3.19-b).

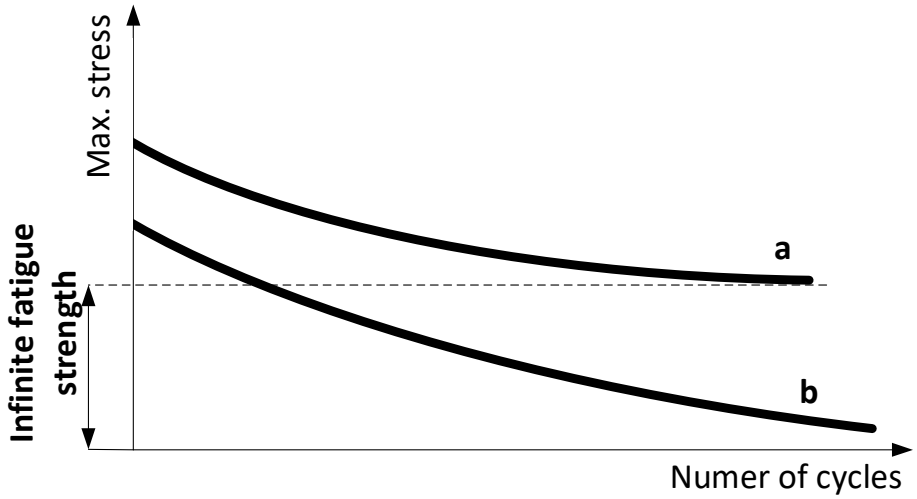

Fig 3.19 Two types of Wöhler curve

The shape and dimensions of samples are determined depending on the type of measured values and the conditions for their determination. Simple-shaped samples are used to determine the Fatigue indices of the materials. In order to determine the fatigue strength of parts and structural elements, samples that provide the fullest possible analogy of the stress distribution and loading conditions. Detailed test guidelines, including standard sample shapes, are provided separately for metals [51, 52], plastics [53, 54] and ceramics [55, 56].

This project has been funded with support from the European Commission. This publication [communication] reflects the views only of the authors, and the Commission cannot be held responsible for any use which may be made of the information contained therein.

4 Introduction to mechanical testing

Characteristic of the technical aspect of a medical product, such as orthoses and prostheses, includes four different areas, which are dimensional inspection, mechanical, climatic and durability tests [57].Mechanical testing of 3D printed prostheses sand orthoses is a significant concern. There are some reports about notable failures where a 3Dprinted elements break while being in active testing by patients [58].Every new project or invention related to medical equipment should be appropriately tested and checked for compliance with the relevant standards. Additive manufacturing is still such a new manufacturing technology that appropriate standards and test methods are just appearing or are still being developed. For this reason, most often, researchers try to adopt other standards or create a unique measurement methodology suited best to their requirements.

Pure mechanical tests are not meant to directly measure the clinical effectiveness of any medical device. However, accurately measured mechanical and biomechanical data can be used to better satisfy the patient specific requirements and comfort. To help clinicians make better use of digital manufacturing, the need for safety testing method of 3D printed medical devices should be fulfilled [59]. A comprehensive framework of the 3D printing procedure that covers the entire process from the initial conception to the final products could drastically change the nowadays way of producing many medical devices [60].

It should also be remembered that 3D printed elements are typically part of an individualized product. Testing these types of solutions with multiple repetitions is significantly more problematic than with repetitive mass-produced components. Also, the additive manufacturing process itself, depending on a specific method, can be controlled by several or even several dozen parameters. Each of them can influence the obtained strength coefficients and the dimensional accuracy of the manufactured element [61].

In general, it can be assumed that in research projects related to additively manufactured medical products, there are 3 stages of research related to mechanical properties:

- The first is related to the testing of standard test samples or smaller product pieces that are most likely to be damaged. In these tests, universal measuring machines with standard equipment are used. The number of test samples in the series is the largest of all phases.
- In the second stage, the entire products are tested. For loading phantoms or unique stands and measuring equipment are used. In this phase, there should be no less than 3 repetitions in a series, and it is also the most common value in scientific publications describing this type of research. Studying a product in its final form makes reliability and acceptability be assessed using two types of mechanical tests: static and dynamic.
- In the last phase, the strength is checked in direct use by the patient. Thanks to this, it is possible to check not only the resistance to limit loads occurring in standard operating

This project has been funded with support from the European Commission. This publication [communication] reflects the views only of the authors, and the Commission cannot be held responsible for any use which may be made of the information contained therein.

conditions but also to assess the fatigue strength. The third phase of testing usually takes much longer than the previous ones. It can last from several days to several months. The test patient usually receives one product or a specific family of structurally similar products.

Later in this chapter, attention is focused on stage two tests examples. They are not as well standardized as stage one tests. But carrying out them involved purely mechanical testing. Hence does not directly endanger the patient and does not require the approval of ethics committees, as is often the case in stage three tests.

4.1 Prosthesis

4.1.1 Upper limb

Hand

Subassemblies of prosthetic hand can be subjected to some ISO standard test [62], a proposed in annexe A the distal tensile test (figure 4.1). Authors of paper [63] use it to test subassembly of body-powered upper-limb prosthesis made of ABS. In this test, a hand is induced to perform a power grip on a 19 mm diameter cylindrical object. The latter is pulled away, forcing the fingers to extend or to break. This determines the maximum load that the prosthesis can withstand without damage.

Fig. 4.1. Schematic draw of hand tensile test [63]

This project has been funded with support from the European Commission. This publication [communication] reflects the views only of the authors, and the Commission cannot be held responsible for any use which may be made of the information contained therein.

As a result of the research, the authors proved that their prosthetic hand could withstand over 112 N of tensile load. The test was conducted using a Zwick Roell Z050 tensile test machine. Some additional, necessary accessories for the test stand have also been printed from ABS material. The complete assembly of the hand tensile test is visible in figure 4.2.

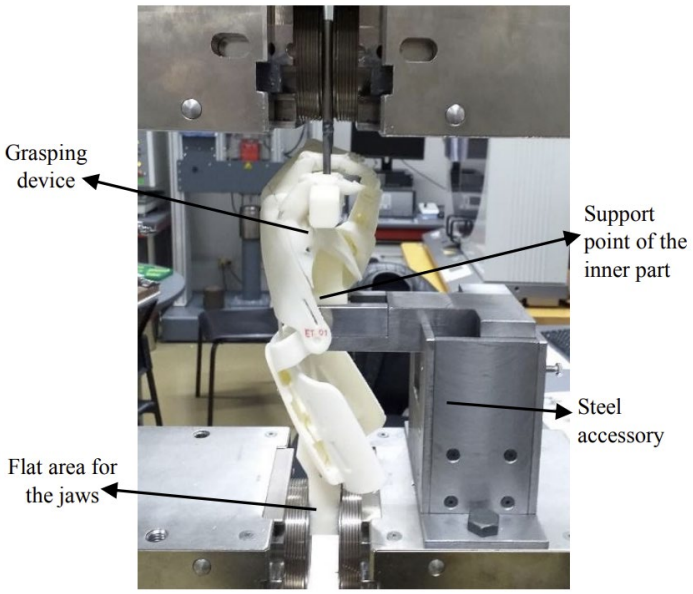

Figure 4.2. Testing stand for prosthetic hand. [63]

The same authors performed two more types of mechanical tests on the fingers of a hand prosthesis. The first one concerned finger flexion and was conducted to evaluate their maximum load-carrying capacity. They used middle and little finger (as the longest and shortest of hand) and extended them in two planes (for hyperextension and abduction simulation). The testing stand was equipped with three additional elements (figure 4.3).

This project has been funded with support from the European Commission. This publication [communication] reflects the views only of the authors, and the Commission cannot be held responsible for any use which may be made of the information contained therein.

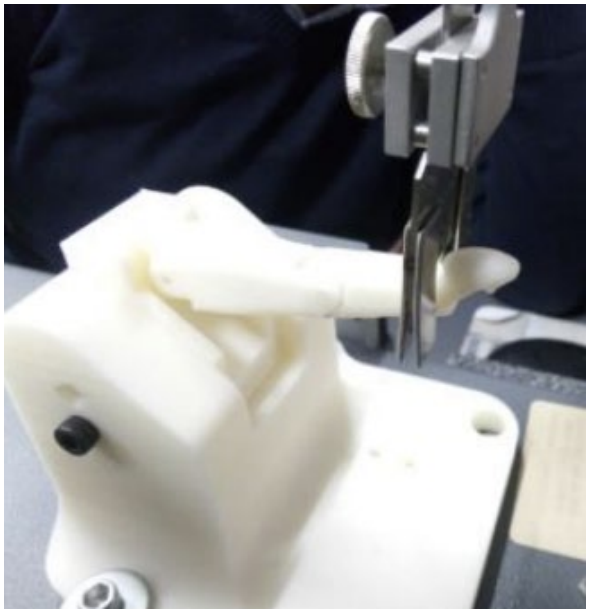

Figure 4.3 Finger flexion test assembly [63]

Other finger tests, described in [63], concerned their fatigue resistance. The authors intended to measure the possible wear between the threads and the internal channels of the prosthesis, as well as metal pins with the flange holes. They used the same testing machine as for the flexural test (Zwick Roell Z0.5), subjecting samples of the index finger to 24000 cycles in flexion mode. This is equivalent to 27 days of the everyday use of the prosthesis [64, 65]. The wear resistance of the assembly was evaluated by weighing the samples before and after the test. All samples showed any signs of failure. The average percentage of variation of weight was 0.05%.As compared to standards material, the authors stated that 3D printed prosthesis parts show a rather low wear rate.

For non-assembly 3D printed hand orthosis presented in paper [66], authors presented experimental setups to measure two mechanical aspects.The first was about leaf spring ultimate strength. As this moving part has the lowest cross-sectional area is most prone to failure. What is more, leaf spring experience combined tensile and bending forces. Proposed by the authors testing setup is presented in figure 4.4. It consisted of an ElectroPuls E10000 (Instron) electrodynamic testing machine and customized 3D-printed PLA samples designed to fit into the testing clamps.

This project has been funded with support from the European Commission. This publication [communication] reflects the views only of the authors, and the Commission cannot be held responsible for any use which may be made of the information contained therein.

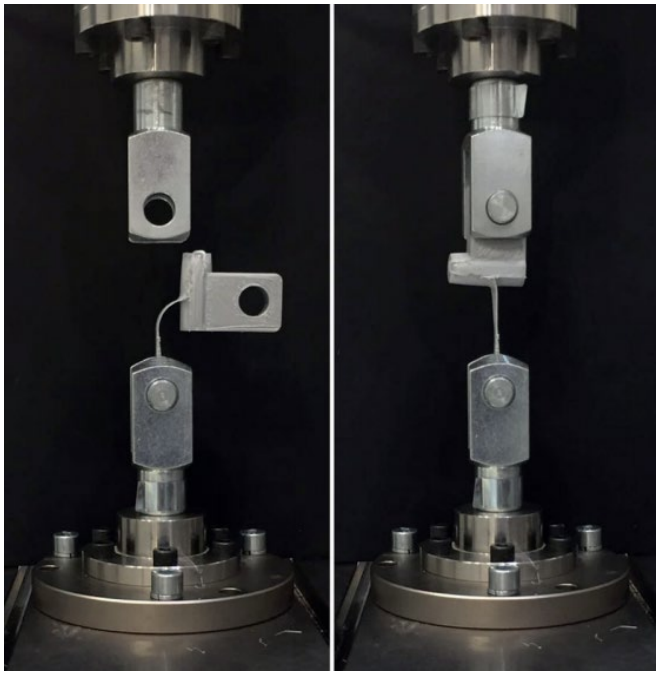

Figure 4.4.The experimental setup for the leaf spring ultimate strength test [66]

The second test was conducted to study the mechanical performance of the prosthetic hand. The test setup measured the input force using a load cell (Zemic: FLB3G-C3-50 kg-6B), the pinch force of the prosthetic hand using 11mmthick cover encasing a FUTEK LLB130 load cell positioned on the tip of the thumb, and the actuation displacements of the driving cable using a displacement sensor. The measurements of the energy input to close the device and the energy returned to move the fingers back to the straight configuration were used to calculate the mechanical efficiency of the hand prosthesis. The test setup is presented in Figure 4.5.

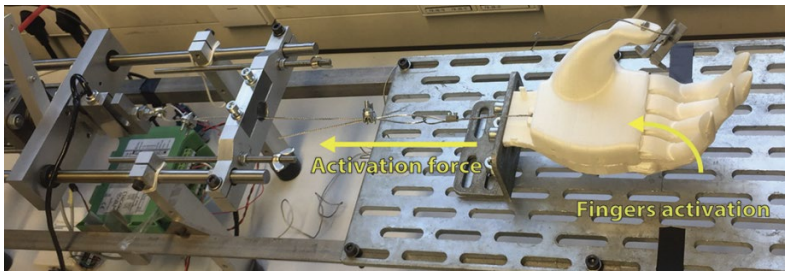

Figure 4.5. The experimental setup to measure the activation and pinch forces [66]

This project has been funded with support from the European Commission. This publication [communication] reflects the views only of the authors, and the Commission cannot be held responsible for any use which may be made of the information contained therein.

Another testing setup to measure prosthetic hands force necessary to close was presented in paper [67]. A platform and some additional elements were needed to secure the gauntlet and expose the hand to be applied to apply a force necessary to close the hand. A screw was attached as well to eliminate slipping on the plastic hand base when in contact with the Instron universal testing machine. The testing set up can be seen in Figure 4.6.

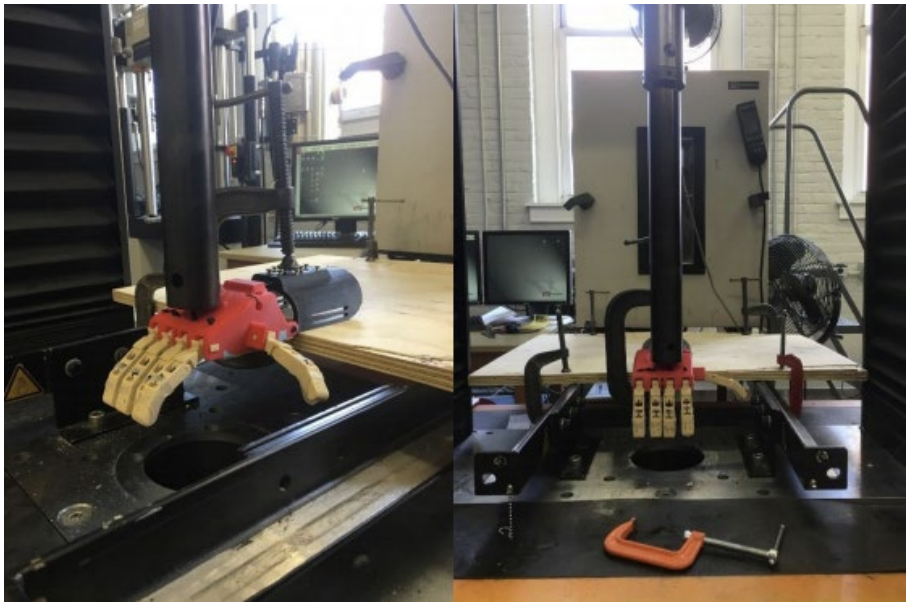

Figure 4.6. Instron setup to measureforce to close prosthetic hand[67]

Sockets

There are no dedicated standards for mechanical testing for 3d-printed upper-limb prosthesis sockets [68]. This is one of the main reason to be difficult to introduce new materials or new methods of prosthesis manufacturing, because it is hard to make a good comparison against traditional materials and production methods.

Most scientific papers presented a new design of 3D printed upper-limb prosthesis use additively manufactured simple samples to determine mechanical properties. Measured data is next use in finite element modelling. In an effort to have consistent and reliable 3D-printed components for use in the medical environment, consistent standards and best practices should be implemented [69].

This project has been funded with support from the European Commission. This publication [communication] reflects the views only of the authors, and the Commission cannot be held responsible for any use which may be made of the information contained therein.

4.1.2 Lower limb

Ankle-foot and foot

There are many different types of foot prostheses. In order to correctly classify and describe them, the authors of the report [70] proposed 10 descriptors and sets of dynamic mechanical testing procedures (exemplary dynamic keel test is presented in Figure 5.7). The authors note that descriptors should be applied only within the context of the prosthetic foot and ankle systems. The mechanical tests require test-specific fixtures to be installed in the material testing machine. The authors of the paper [71] confirmed that these test outcomes are reliable and repeatable. There are reportedthe following outcome metrics and associated test:

a) Vertical Linear Displacement - Vertical loading and unloading of foot onto 20° sagittal-plane inclined surface.
b) Vertical Energy Return - Vertical loading and unloading of the foot onto 20° sagittal-planeinclined surface.
c) Vertical Linear Displacement - Vertical loading and unloading of the foot onto 15° sagittal-planedeclined surface.
d) Vertical Energy Return - Vertical loading and unloading of the foot onto 15° sagittal-planedeclined surface.
e) Coronal-Plane Angular Displacement - Vertical loading (medial biased plantar force vector) andunloading of foot fixed in cradle with free coronal-plane rotation.
f) Transverse-Plane Angular Displacement -Transverse-plane torque loading and unloading applied to foot and pylon constrained by the fixed end andopposing end with free transverse-plane rotation.
g) Vertical Linear Displacement - Vertical loading and unloading of foot and pylononto sagittal-plane level surface.
h) Vertical Linear Displacement - Sagittal-plane torque loading and unloadingapplied to the distal end of foot and pylon (i.e., cantilever load scenario).
i) Horizontal Linear Displacement - Vertical loading and unloading of foot angled at 15° dorsiflexion onto sagittal-plane level surfacewith free sagittal-plane linear translation.
j) Horizontal Linear Displacement - Vertical loading and unloadingof foot angled at 20° plantarflexion onto sagittal-plane level surfacewith free sagittal-plane linear translation.

This project has been funded with support from the European Commission. This publication [communication] reflects the views only of the authors, and the Commission cannot be held responsible for any use which may be made of the information contained therein.

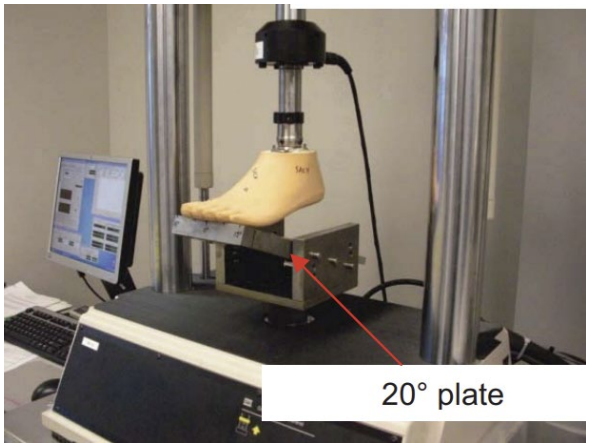

Figure 4.4. Dynamic keel test used to measure Vertical Linear Displacement and Vertical Energy Return [70]

In paper [72] compression tests of low cost, 3D-printed foot are presented. The prototype made of ABS was tested twice. In the first attempt was placed on its sole without additional support. A 600 N force was applied three times, with the loading rate 0.5 mm/min, 1 mm/min and 1.5 mm/min

respectively. In the second test five different loads were applied in increasing order: 200 N, 400 N, 600 N, 800 N and 1000 N respectively, while loading rate was constant at 1 mm/min. What is more, greater forces required extra support at the heel to avoiding undesired slipping, to be applied. The authors used Instron 5965 testing machine (Figure 4.8). In the paper, any ISO standard is mentioned. The presented result shows that the measured prototype failed at approximately 850 N and the yield point was at 750 N. Hence usability of such prosthetic foot is limited for moderate activity patients. The authors concluded that the development of a novel 3D printed prosthesis is limited to the material and not to the design. They indicated that for high activity level patient Continues Filament Fabrication (CFF) method could give much better results.

This project has been funded with support from the European Commission. This publication [communication] reflects the views only of the authors, and the Commission cannot be held responsible for any use which may be made of the information contained therein.

Figure 4.8. Prosthetic ABS foot compression test setup [72]

A CFF method was used, by other authors, to manufacture 3D printed prosthetic foot [73]. They test it under two conditions (keel and heel test) according to the standard ISO 22675 [74]. The keel should have the capability of energy storage and return during walking, and the heel should have a stiffer behaviour that gives balance to the patients [75].The foot could recover its original shape without visible fractures under loads greater than 4000 N. Used test setup is presented in Figure 4.9.

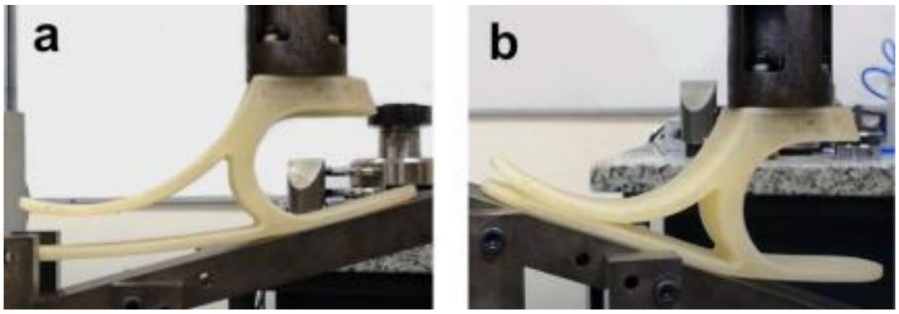

Figure 4.9 Maximum deformation of the prosthetic foot in heel test (a) and keel test(b) [73]

This project has been funded with support from the European Commission. This publication [communication] reflects the views only of the authors, and the Commission cannot be held responsible for any use which may be made of the information contained therein.

In the case of a 3D printed transtibial prosthesis, complete sets and sockets (Figure 4.10),researchersverify the safety of the product and its part using a variety of different mechanical tests, such as compressive axial test and pure bending tests. Nevertheless, without official standard associated with theses test in scope of the transtibial prosthesis, it is rather tricky to unequivocally specify if those type of product is safe to end-user [76].

Figure 4.10. Example of transtibial prosthesis (3D-printed on the left side of the figure and conventional on the right) [77]

A more suitable assessment of the conformity could be done using the International Standard ISO-10328. It specifies many types of procedures for static and cyclic strength tests on lower-limb prostheses. These tests simulate either the heel strike or the toe-off portion of a typical step taken by people. Measured loads are related to the peak values of the components of loading, which generally occur during the stance phase of walking [76, 78].

The test can be performed with a typical static test machine, and a 5 kN load cell is enough to simulate the magnitude of the force that may appear during normal use of lower limb prostheses. In testing procedures, which are not intended to damage prosthetic socket, the most common load is the equivalent of the single-limb stance load exerted by a person with a weight in the range from 75 kg to

This project has been funded with support from the European Commission. This publication [communication] reflects the views only of the authors, and the Commission cannot be held responsible for any use which may be made of the information contained therein.

125 kg.In destructive testing,3d-printed sockets usually break at the interface of the layers. For example, sockets made with FDM method of polypropylene composite (PP) material reinforced with microfibrillated cellulose (MFC), depending on the printing direction, were damaged when loaded with a force from 1343 to 2896 N [77]. The authors of the system for custom-fit sockets named SocketMixer [79] showed that 3D printed sockets could withstand twice the estimated jumping load of the 18-years-old patient (4500 N).

Prosthesis socket test requires the application of a force that is not perfectly aligned with the axis of the static test machine. To simulate the worst possible conditions for normal use of the lower limb prosthesis, the socket must be subjected to simultaneous compression, off-axial bending and torsion. For this reason, it is necessary to use special equipment that will interface with the test machine and the socket. Different sockets, along with dedicated hardware for force transmission, is shown in Figure 4.11.

Figure 4.11. Exemplary testing stands for transtibial prosthesis [76, 77]

Sockets can only be loaded with a single load or be loaded cyclically. In the latter case, an iterative force loading is sometimes used, which increases with each successive cycle. The minimum number of

This project has been funded with support from the European Commission. This publication [communication] reflects the views only of the authors, and the Commission cannot be held responsible for any use which may be made of the information contained therein.

repetitions of samples in the series should not be less than 3, which make it possible to assess the repeatability of the results.

To make the test conditions even more realistic, the prosthesis should be loaded with a dedicated residual limb phantom (Figure 4.12). It should be strong enough to sustain high testing loads without any damage. The initial fitting of the phantom with the socket is performed with a force of up to 50 N[80]. Phantom should have two parts to better mimic human limb. The inner, more rigid core, imitating bones, should have shore hardness between 65A and 85A [81]. While softer, outer shell, should have shore hardness imitating skin (00-30A) and muscles (10-50A) [63].Moreover, a prosthetic liner and a nylon stocking should be placed between the socket and the residual limb phantom [80].

Figure 4.12. Photo of two residual limb phantoms, taken prior to any testing [80]

A standardized method of testing prosthetic liners used in lower-limb prosthetics was proposed by the authors of [82]. They characterized the liners on the basis of a set of six material parameters. The described method could also be applied to inserts made with the help of 3D printing.

Transfemoral

The test methodsfor feet, pylons and transfemoral socketsare similar or the same as that of transtibial ones.

The authors of the study [83] conclude that the use of additive manufacturing to build transfemoral prostheses makes them larger and heavier than warranted. Especially manufacturing via the most common method of Fused Deposition Modeling runs into the problem of being excessively anisotropic. Hence manufactured parts of prosthesis tends to de-lamination along withspecific directions. This

This project has been funded with support from the European Commission. This publication [communication] reflects the views only of the authors, and the Commission cannot be held responsible for any use which may be made of the information contained therein.

property of FDM products should always be kept in mind when designing a new geometry and testing prototypes.

Hip

There are people who live without any limbs from the hip to the joint downwards. The only possibility of their locomotion is use of devices like wheelchairs or hip disarticulation prostheses [84]. The test conditions for the latter are specified by the ISO 15032 standard [85]. However, there are no documented cases of using this standard for the testing of prostheses made with the use of 3D printing in the scientific literature.

4.2. Orthoses

4.2.1 Upper limb

Hand

Post-stroke patients could have problem with finger spasm. To support their rehabilitation, a hand orthosis could be applied. The geometry of the orthosis personalized for each patient enables better spasm relief. The designing process may include scanning of a healthy hand and ultimately leads to a product with an appearance similar to that shown in Figure 4.13.

Figure 4.13. Model of post-stroke hand orthosis [86]

In the paper [86], the authors concluded that the most important strength aspect of the hand orthosis is flexural strength. They carried out a bending test of the middle fingers of the hand. All measured bending forces for all used materials - photopolymer (317 N), policarbon (143N) and acrylo-butadieno-styrene (95 N) - were greater than patient muscle tone (49 N). On this basis, they

This project has been funded with support from the European Commission. This publication [communication] reflects the views only of the authors, and the Commission cannot be held responsible for any use which may be made of the information contained therein.

constructed the finite element model, which proved that even the least durable ABS material could be applied to the clinical rehabilitation treatment. The model can be reused for other patient's hand models and optimization of the geometry with regard to the wall thickness of the orthosis.

Wrist-hand

Post-stroke patients use on a home-based therapy manner an anti-spastic wrist-hand orthosis. This type of product helps them to enhance the upper limb functions. Such orthosis can be made by forming a warm laminate plate directly on the patient limb, to which in the next step, a 3D printed framework is attached. To separate skin from heat, authors of paper [87] proposed folded layers of flexible thermoplastic polyurethane (TPU). They characterize the thermal properties of 3D printed TPU coatings and performed a flex resistance test on test specimens, according to ISO 32100 standard [88].

The paper [89] presents the results of research conducted on a batch of additively manufactured individualized orthoses made of thermoplastics with FDM method. Their experiments focused on the selection of materials and parameters of an additive manufacturing process ofthe openwork wrist–hand orthosis designed fully automatically based on a 3D scan of a given patient. Destructive testing consisted of a quasi3-point bending test of the whole orthosis (Figure 4.14).To simulate bending with a patient's hand inside ,a two-material forearm phantom was manufactured. The shell was made of TPU (elastic thermoplastic polyurethane) material, infill 15%, the core was made of ABS, infill 30%. The strength tests were performed with the universal strength testing machine SunpocWDW-5D-HS (Sunpoc, Guiyang, China). The course of the experiment was developed based on ISO527-2:2012 standard [90].Specially shaped supports were designed and manufactured out of ABS material and placed and screwed to thetest machine's rail, 40–50 mm far from the load. During loading, the orthosis was not additionally fixed—the supports significantly limited the freedom of movement of the product (Fig. 31).The test was carried out until an orthosis was destroyed (by cracking) or visibly deformed. As a threshold of positive evaluation of a given orthosis, a load of 300 N was assumed(representing a static bending using an item of 30 kg mass). The value was set arbitrarily, based on the discussion in the project team, with mechanical and biomedical engineers and with expert participation of orthopedists and physiotherapists, who stated that in practice, such orthoses do not need to bear higher loads. Analyzing the collected results, the authors concluded that to recommend regular users to select the PLA material if they do not predict the orthosis suffering dynamic loads or higher temperatures—in such case, ABS is recommended. If the orthosis must bear higher loads, be temperature-resistant, partially elastic and skin-friendly, nylon is recommended, but at higher costs [89].

This project has been funded with support from the European Commission. This publication [communication] reflects the views only of the authors, and the Commission cannot be held responsible for any use which may be made of the information contained therein.

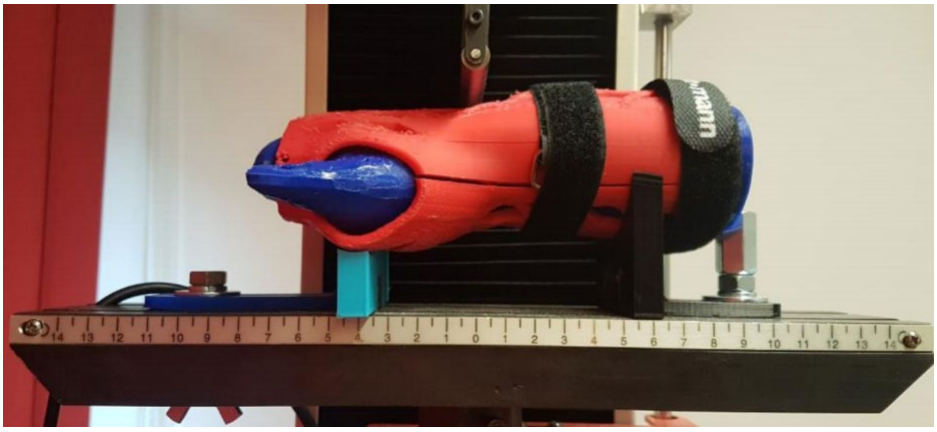

Figure 4.14. Bending test of an orthosis with a forearm phantom [89]

4.2.2 Lower limb

Foot

Foot orthoses which are fabricated using 3D printer, has their geometry acquired by 3D scanning of the user foot and are dedicated to fully or partially cover the medial and lateral longitudinal arch of the foot. As stated authors of the paper [91], there is no standard test to obtain the mechanical characteristic of the foot orthoses. They propose to fix orthoses with the rectangular fixture placed on the lateral side. Then subject it to dynamic compression at a constant loading speed of 105 N/min by a standard testing machine equipped with a 40 mm diameter indenter (Figure 4.15).

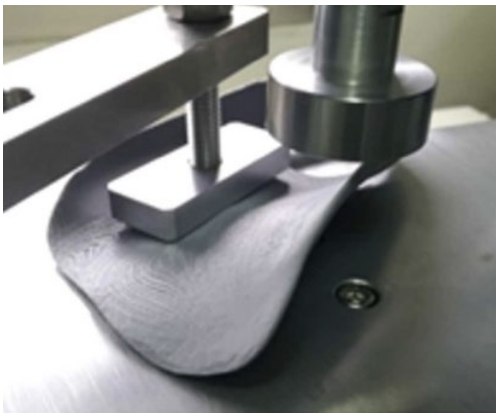

Figure 4.15. Foot orthoses testing stand [80]

This project has been funded with support from the European Commission. This publication [communication] reflects the views only of the authors, and the Commission cannot be held responsible for any use which may be made of the information contained therein.

Ankle-foot

Manufacturers of standard orthoses who want to comply with ISO 22523 [62] need to inform about required strength and attendant test methods. Nevertheless, there is not clearly defined the test load of the test method [92].The analysis of available scientific studies shows that the orthoses, as well as their usefulness and reliability, are checked in two types of tests - static and dynamic. The formers are carried to find out the maximum load a medical device could sustain. The range of force that needs to be supported by a standing adult person who is using ankle-foot orthosis is from 180 to 900 N and depends on measurement point and way of usage [93]. The stiffness of the orthosis is also indicated as an essential feature, measured in the static test, as it affects not only its general usability but also wear resistance [94]. The dynamic tests of orthosis are necessary in the scope of the biomechanics of gait. They usually take the form of clinical investigation. During the tests, people from certain groups walk with different types of AFO under appropriate conditions [95]. Information obtained on the basis of tests can be used in computer models and simulation studies [96].

The authors of the paper [97] noted that with no routine objective method for mechanical testing of 3D printed AFO orthosis, most of the literature examples have their own specific setups. The most common setups utilized a dedicated bench, hence they are difficult to replicate, thus reduce options for direct clinical applications. The literature review indicated the following measurement possibilities for ankle-foot orthosis:

- Elastic properties (a measure of devices' ability to exhibit any permanent deformation after a force is applied)
- Angular deflection, by calculating stiffness around the ankle
- Failure under compressive forces (dorsiflexion moment).

In Figure 4.16 a testing setup for ankle-foot orthosis is presented. It was designed for representing the gait cycle from initial conduct until toe off. All tests were set out to first replicate plantarflexion (tension) and then dorsiflexion (compression) moments: force initially to the heel and subsequently to the forefoot. The authors kept testing procedures with ISO guidelines [98]. The authors managed to obtain interesting results but highlighted in the summary of their work, that it is recommended that International Standards be established. As a result, it would be possible to directly compare of different products, where many claims to perform the same function without comparable evidence [97].

This project has been funded with support from the European Commission. This publication [communication] reflects the views only of the authors, and the Commission cannot be held responsible for any use which may be made of the information contained therein.

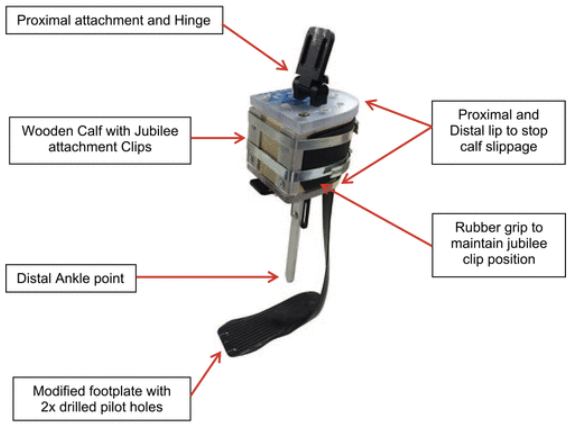

Figure 4.16. Ankle-foot orthosis testing setup proposed by authors [97]

Anterior type of ankle-foot orthoses (AAFOs) is an AFO type more suitable for walking. In paper [96] a comparison between 15 traditionally made and 15 3D printed AAFOs is presented. The former was made of thermoplastic polypropylene. The latter was made of PLA with the use of FFF method. The authors conducted mechanical tests using HT-2402Material Testing Machine from Huang-ta Co. Ltd. The intender, visible in Figure 4.17, applied force to samples with a constant rate of 20 N/min. All samples were loaded until break or end of displacement range to measure ultimate strength. No standard was applied to these tests. Most of the 3D printed AAFOs were fractured on the neck. They were stiffer than traditionally made AAFO's, but the latter showed greater flexibility and ductility, as no fracture was observed.

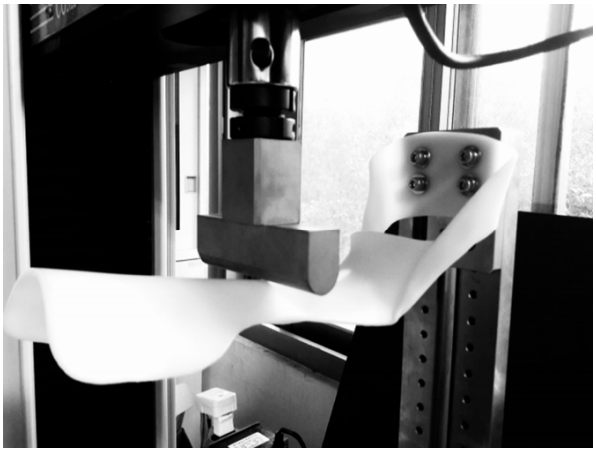

Figure 4.17. Mechanical testing of the AAFO in the simulation of plantarflexion [99]

This project has been funded with support from the European Commission. This publication [communication] reflects the views only of the authors, and the Commission cannot be held responsible for any use which may be made of the information contained therein.

In Figure 4.18, the stand for AFO durability test is presented. At both ends of the AFO, made of thermoplastic polyurethane, round-shaped plastic dummies were inserted and affixed to the machine. Cycling loading force of 50 N was applied with a frequency of 1 Hz. In the authors' opinion, this simulated the partial bodyweight to endure the stance phase and the cadence of walking. A total of 300000 cycles represent 4 months of patients activity. There was no crack or damage after all repetitions. After the durability test, the shape and stiffness of the AFO did not change [100].

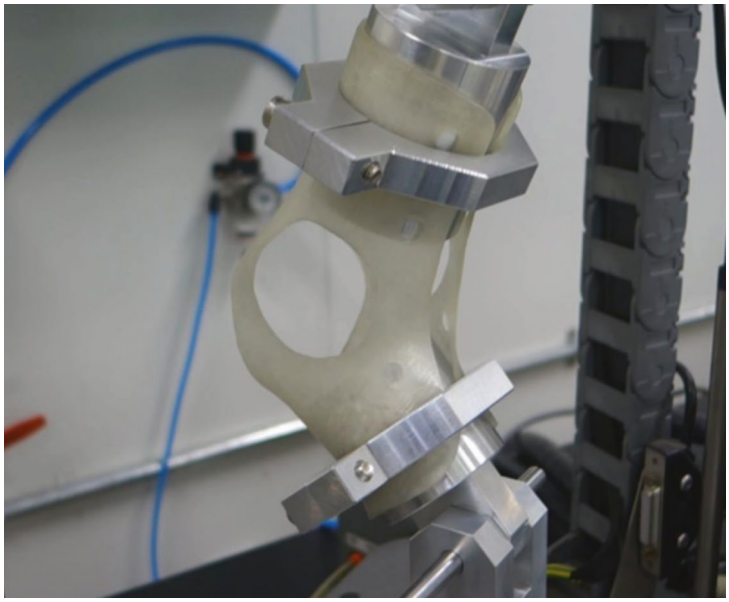

Figure 4.18. AFO durability test stand [100]

This project has been funded with support from the European Commission. This publication [communication] reflects the views only of the authors, and the Commission cannot be held responsible for any use which may be made of the information contained therein.

5 Methods of non-destructive testing of materials produced with RP techniques

5.1. Scanning Electron Microscopy (SEM)

Introduction

Using a directed beam of high-energy electrons, a scanning electron microscope (SEM) can image topography and acquire material details on conductive specimens. Since its development in the 1930s, by Ernst Ruska and Max Knoll, the fundamental nature and philosophy of the electron microscope (EM) has changed little. However, over the decades even as prices have declined, gradual improvements in power and resolution were obtained. Recent developments in EM-technology led, in particular, to a revival in the last 10 years, of the use of the scan electron microscopy in biological science. More recent developments in the imagery of a tissue block after iterative removal of ultrathin (10 nm–50nm) parts of the tall layer using an ultra-microtome incorporated into the EM have allowed neural tissue images to be reconstructive, which enables scientists to investigate neurons and their connections in detail.

The general principles

Scanned Electron Electron Microscopes operate in similar ways to optical microscopes, except that the electrons use a directed light beam to "image" the specimen and collect information on the structure and nature of the specimen. The unaided human eye can distinguish 2 points 0,2 mm apart, given enough lighting. If the points are closer together, they are a single point. This difference is known as the eye's resolution or resolution. Similarly, light-emitting microscopes use light (400-700nm) and lenses for small specimens, such as a red blood cell (7 m) or human hair (a millionth of one metre) (100 m). The magnification of a light microscope is about 1000x, enabling the eye to solve 200 nm divided structure. In response to light microscopic shortcomings which are restricted by light physics, electron microscopes were developed. Electron microscopes have substantially higher magnifications and resolution capacity compared with light microscopes, enabling them to see significantly clearer subcellular, biological, and atomic structures. In the case of the wavelength of the illuminating source, the resolution of the microscope is most effective. The electron gun at the top of the transmission electron microscope illuminates the specimen, and the condenser lens controls the beam angle. The lenses under the specimen magnify the image of the specimen, which is then viewed on the final screen at a magnification of thousands of times. If a second electron gun is mounted under the fluorescent screen at the bottom of the column and the electron beam is reflected upwards using the same lenses as the first, the size of the second electron source would be decreased by the same amount as the specimen image is magnified. For both electron guns on at the same time, this result can be shown, demonstrating the reversibility of rays through electron lens systems. In this way, the oriented electron probe in the plane of the specimen is equal to the resolved point in the specimen picture on the fluorescent screen or on the photographic plate. The working principle can be seen on picture 5.1 and 5.2.

This project has been funded with support from the European Commission. This publication [communication] reflects the views only of the authors, and the Commission cannot be held responsible for any use which may be made of the information contained therein.

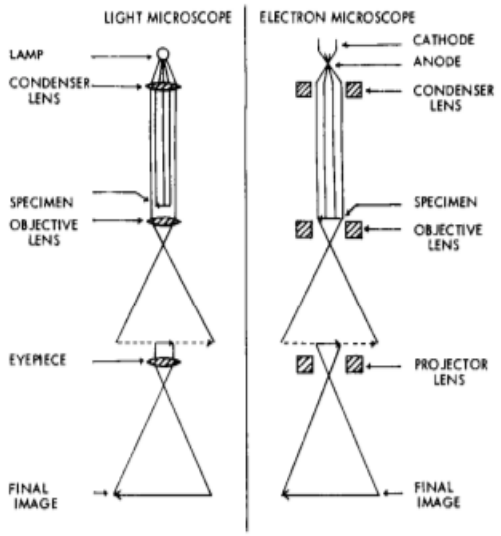

Figure 5.1. Working principle of SEM [101]

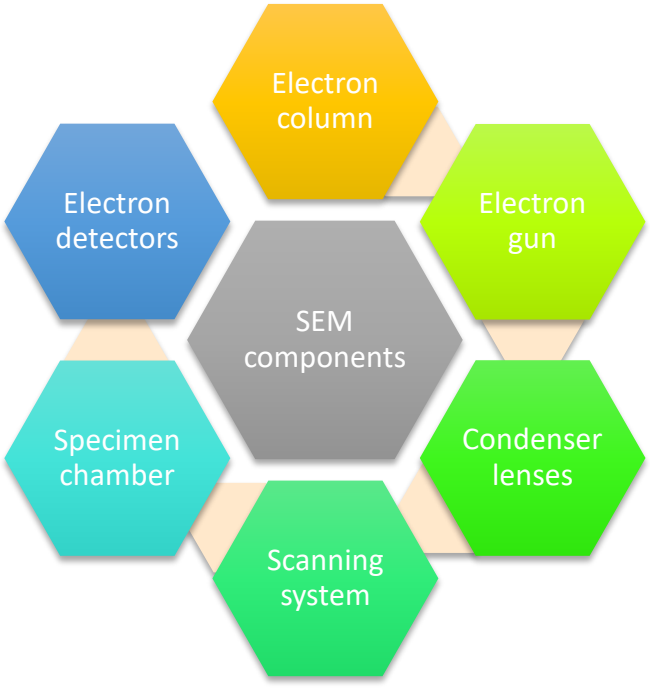

Figure 5.2. Main SEM components overview

This project has been funded with support from the European Commission. This publication [communication] reflects the views only of the authors, and the Commission cannot be held responsible for any use which may be made of the information contained therein.

Applications of SEM system

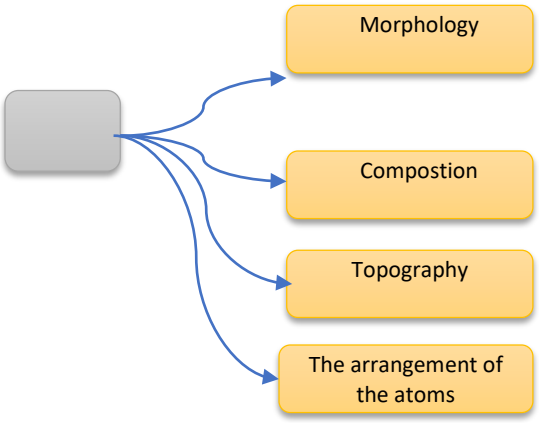

5.2 Atomic force microscopy (AFM)

Atomic force microscopy (AFM) is a type of scanning probe microscopy (SPM), with demonstrated resolution on the order of fractions of a nanometer, more than 1000 times better than the optical diffraction limit (figure 5.3). The information is gathered by "feeling" or "touching" the surface with a mechanical probe. Piezoelectric elements that facilitate tiny but accurate and precise movements on (electronic) command enable precise scanning.

The AFM has three major abilities: force measurement, topographic imaging, and manipulation.

In force measurement, AFMs can be used to measure the forces between the probe and the sample as a function of their mutual separation. This can be applied to perform force spectroscopy, to measure the mechanical properties of the sample, such as the sample's Young's modulus, a measure of stiffness.

For imaging, the reaction of the probe to the forces that the sample imposes on it can be used to form an image of the three-dimensional shape (topography) of a sample surface at a high resolution. This is achieved by raster scanning the position of the sample with respect to the tip and recording the height of the probe that corresponds to a constant probe-sample interaction (see section topographic imaging in AFM for more details). The surface topography is commonly displayed as a pseudocolor plot. Although the initial publication about the atomic force microscopy by Binnig, Quate and Gerber in 1986 speculated about the possibility of achieving atomic resolution, profound experimental challenges needed to be overcome before atomic resolution of defects and step edges in ambient (liquid) conditions was demonstrated in 1993 by Ohnesorge and Binnig [102]. True atomic resolution of the silicon 7x7 surface - the atomic images of this surface obtained by STM had convinced the scientific community of the spectacular spatial resolution of scanning tunneling microscopy – had to wait a little longer before it was shown by Giessibl [103].

This project has been funded with support from the European Commission. This publication [communication] reflects the views only of the authors, and the Commission cannot be held responsible for any use which may be made of the information contained therein.

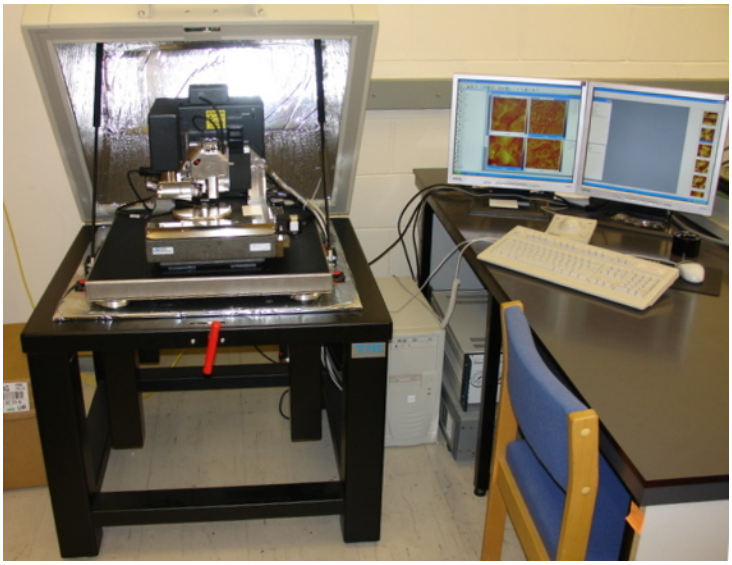

Figure. 5.3. An atomic force microscope on the left with controlling computer on the right [104]

In manipulation, the forces between tip and sample can also be used to change the properties of the sample in a controlled way. Examples of this include atomic manipulation, scanning probe lithography and local stimulation of cells.

Simultaneous with the acquisition of topographical images, other properties of the sample can be measured locally and displayed as an image, often with similarly high resolution. Examples of such properties are mechanical properties like stiffness or adhesion strength and electrical properties such as conductivity or surface potential. In fact, the majority of SPM techniques are extensions of AFM that use this modality.

Figure 5.3 shows an AFM, which typically consists of the following features. Numbers in parentheses correspond to numbered features in Figure 5.4. Coordinate directions are defined by the coordinate system (0).

This project has been funded with support from the European Commission. This publication [communication] reflects the views only of the authors, and the Commission cannot be held responsible for any use which may be made of the information contained therein.

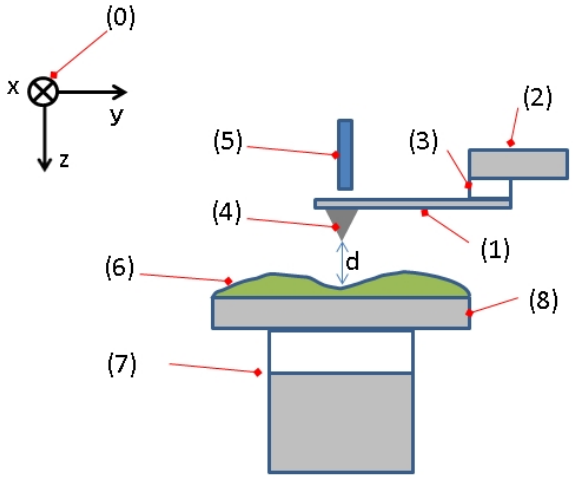

Figure 5.5. Typical configuration of an AFM, (1): Cantilever, (2): Support for cantilever, (3): Piezoelectric element (to oscillate cantilever at its eigen frequency), (4): Tip (Fixed to open end of a cantilever, acts as the probe), (5): Detector of deflection and motion of the cantilever, (6): Sample to be measured by AFM, (7): xyz drive, (moves sample (6) and stage (8) in x, y, and z directions with respect to a tip apex (4)), and (8): Stage. [105]

The small spring-like cantilever (1) is carried by the support (2). Optionally, a piezoelectric element (typically made of a ceramic material) (3) oscillates the cantilever (1). The sharp tip (4) is fixed to the free end of the cantilever (1). The detector (5) records the deflection and motion of the cantilever (1). The sample (6) is mounted on the sample stage (8). An xyz drive (7) permits to displace the sample (6) and the sample stage (8) in x, y, and z directions with respect to the tip apex (4). Although Fig. 5.4 shows the drive attached to the sample, the drive can also be attached to the tip, or independent drives can be attached to both, since it is the relative displacement of the sample and tip that needs to be controlled. Controllers and plotter are not shown in Figure 5.4.

Sample of AFM shows topographical scan of a glass surface show Figure 5.5.

This project has been funded with support from the European Commission. This publication [communication] reflects the views only of the authors, and the Commission cannot be held responsible for any use which may be made of the information contained therein.

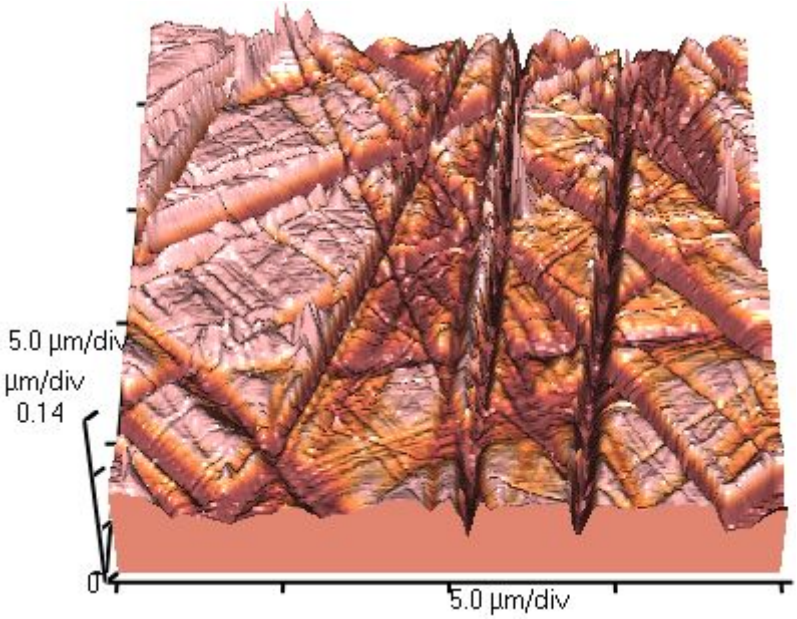

Figure 5.5. Atomic force microscope topographical scan of a glass surface. The micro and nano-scale features of the glass can be observed, portraying the roughness of the material. The image space is (x,y,z) = (20 µm × 20 µm × 420 nm) [105]

5.3 Transmission Electron Microscopy (TEM)

Transmission electron microscopy (TEM) is a microscopy technique in which a beam of electrons is transmitted through a specimen to form an image (figure 5.6). The specimen is most often an ultrathin section less than 100 nm thick or a suspension on a grid. An image is formed from the interaction of the electrons with the sample as the beam is transmitted through the specimen. The image is then magnified and focused onto an imaging device, such as a fluorescent screen, a layer of photographic film, or a sensor such as a scintillator attached to a charge-coupled device.

The most important element of the transmission electron microscope is the microscope column (1), which contains an electron gun (2) generating (e.g. as a result of thermo-emission or field emission) an electron beam (3). The pre-formed electron beam in the area between the cathode (4) and the anode (5) is accelerated to obtain the energy: $E = eU$, where e is the charge of the electron and U is the voltage between the cathode and anode.

Increasing the voltage allows the electron momentum to be increased, which reduces the wavelength. For example, when the accelerating voltage U = 300 kV, then the electron wavelength λ = 0.00197 nm. For this voltage, the speed of electrons in the microscope column v = 0.776 c, where c is the speed of light in a vacuum. In order for the electrons to travel from the electron gun to the screen, it is necessary to maintain a very high vacuum in the column. The optical lenses are matched by a suitably shaped magnetic field that changes the course of the electrons in the focusing coils (6). An

This project has been funded with support from the European Commission. This publication [communication] reflects the views only of the authors, and the Commission cannot be held responsible for any use which may be made of the information contained therein.

important advantage of magnetic lenses is the ability to smoothly change their focal lengths by regulating the intensity of the current flowing through the lens.

When an accelerated electron beam hits a specimen, a number of effects occur that are used in various research devices. In the case of sufficiently thin specimens, some of the electrons pass through the specimen (7) and are used in transmission electron microscopes.

The electrons can be reflected from the specimen or they can knock out electrons from the specimen, called secondary. These two types of electrons are used in reflection microscopes. The electrons falling on the specimen may also excite electrons of the atoms of the tested sample, which then emit X-ray radiation characteristic of the sample atoms. Many electron microscopes, both transmission and scanning, are equipped with one or more EDS (energy dispersive X-ray spectroscopy) or WDS (wavelength dispersive X-ray spectrometry) spectrometers, allowing for chemical composition analysis samples.

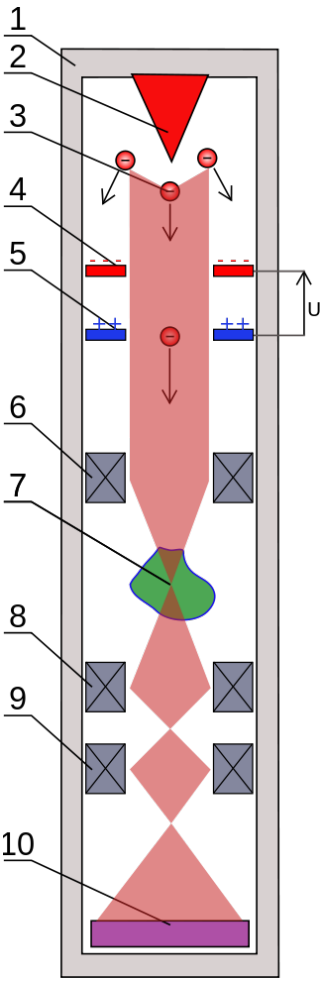

After passing through the specimen, the electron beam can be shaped like light rays, using the lens (8) - eyepiece (9) system. In the case of electrons, instead of glass optical elements, coils are used to change the course of the charged particles. The microscope can work in the image mode, then the beam creates an image of the specimen on the detector (10). The microscope working in the diffraction mode may not have the objective coils and the eyepiece, the image is formed by electrons as a result of the phenomenon of diffraction on the sample structure. In the first constructions, the detector was an electron-luminescent screen (now also used), in the current constructions the detector in the form of a CCD matrix, stimulated by electrons, allows reading the image as electrical signals, and the appropriate measuring apparatus allows for recording information and creating an image of the sample.

Figure 5.6. A simplified diagram
of a transmission electron microscope [106]

The transmission electron microscope allows you to observe the structure of animate and inanimate matter. Thanks to this, we can learn about the structure of animal and plant cells, as well as the structure of minerals, metals and plastics (figure 5.7). Due to the high vacuum in the microscope chamber, the test object must be properly prepared.

This project has been funded with support from the European Commission. This publication [communication] reflects the views only of the authors, and the Commission cannot be held responsible for any use which may be made of the information contained therein.

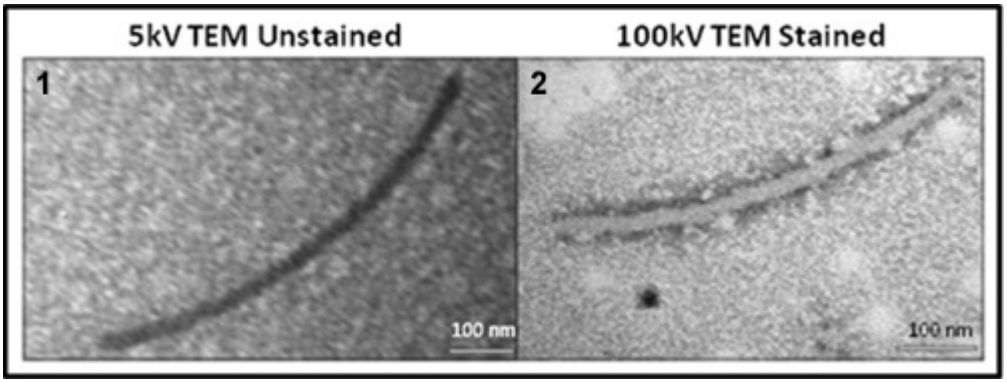

Figure 5.7. Sample of TEM scan [107]

5.4. Optical microscopy

The optical microscope, also referred to as a light microscope, is a type of microscope that commonly uses visible light and a system of lenses to generate magnified images of small objects. Optical microscopes are the oldest design of microscope and were possibly invented in their present compound form in the 17th century. Basic optical microscopes can be very simple, although many complex designs aim to improve resolution and sample contrast.

The object is placed on a stage and may be directly viewed through one or two eyepieces on the microscope. In high-power microscopes, both eyepieces typically show the same image, but with a stereo microscope, slightly different images are used to create a 3-D effect. A camera is typically used to capture the image (micrograph).

The sample can be lit in a variety of ways. Transparent objects can be lit from below and solid objects can be lit with light coming through (bright field) or around (dark field) the objective lens. Polarised light may be used to determine crystal orientation of metallic objects. Phase-contrast imaging can be used to increase image contrast by highlighting small details of differing refractive index (Figure 5.9).

This project has been funded with support from the European Commission. This publication [communication] reflects the views only of the authors, and the Commission cannot be held responsible for any use which may be made of the information contained therein.

Figure 5.8. High resolution imaging [108]

A range of objective lenses with different magnification are usually provided mounted on a turret, allowing them to be rotated into place and providing an ability to zoom-in. The maximum magnification power of optical microscopes is typically limited to around 1000x because of the limited resolving power of visible light. The magnification of a compound optical microscope is the product of the magnification of the eyepiece (say 10x) and the objective lens (say 100x), to give a total magnification of 1,000×. Modified environments such as the use of oil or ultraviolet light can increase the magnification (Figure 5.9).

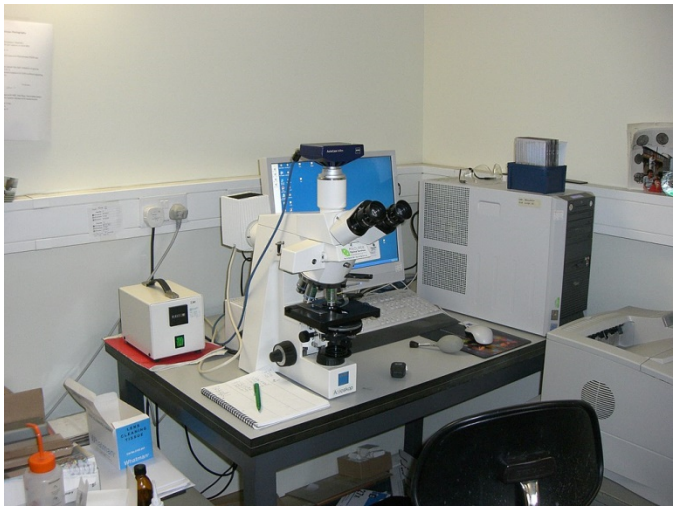

Figure 5.9. A modern optical microscope with a mercury bulb for fluorescence microscopy. The microscope has a digital camera which is connected to a computer [109].

Alternatives to optical microscopy which do not use visible light include scanning electron microscopy and transmission electron microscopy and scanning probe microscopy and as a result, can achieve much greater magnifications.

This project has been funded with support from the European Commission. This publication [communication] reflects the views only of the authors, and the Commission cannot be held responsible for any use which may be made of the information contained therein.

5.5. Energy-Dispersive X-Ray Spectroscopy (EDX / EDS)

Energy-dispersive X-ray spectroscopy (EDS, EDX, EDXS or XEDS), sometimes called energy dispersive X-ray analysis (EDXA or EDAX) or energy dispersive X-ray microanalysis (EDXMA), is an analytical technique used for the elemental analysis or chemical characterization of a sample. It relies on an interaction of some source of X-ray excitation and a sample. Its characterization capabilities are due in large part to the fundamental principle that each element has a unique atomic structure allowing a unique set of peaks on its electromagnetic emission spectrum [110] (which is the main principle of spectroscopy). The peak positions are predicted by the Moseley's law with accuracy much better than experimental resolution of a typical EDX instrument.

To stimulate the emission of characteristic X-rays from a specimen (Figure 5.10) a beam of electrons is focused into the sample being studied. At rest, an atom within the sample contains ground state (or unexcited) electrons in discrete energy levels or electron shells bound to the nucleus. The incident beam may excite an electron in an inner shell, ejecting it from the shell while creating an electron hole where the electron was. An electron from an outer, higher-energy shell then fills the hole, and the difference in energy between the higher-energy shell and the lower energy shell may be released in the form of an X-ray. The number and energy of the X-rays emitted from a specimen can be measured by an energy-dispersive spectrometer. As the energies of the X-rays are characteristic of the difference in energy between the two shells and of the atomic structure of the emitting element, EDS allows the elemental composition of the specimen to be measured.

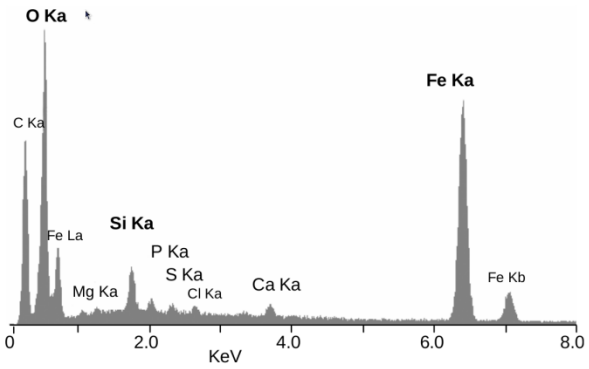

Figure 5.10. EDS spectrum of the mineral crust of the vent shrimp Rimicaris exoculata Most of these peaks are X-rays given off as electrons return to the K electron shell. (K-alpha and K-beta lines) One peak is from the L shell of iron [111].

This project has been funded with support from the European Commission. This publication [communication] reflects the views only of the authors, and the Commission cannot be held responsible for any use which may be made of the information contained therein.

5.6 Diffractometer analysis / X-ray Powder Diffraction (XRD)

A diffractometer produces electromagnetic radiation (waves) with known wavelength and frequency, which is determined by their source. The source is often x-rays, because they are the only kind of energy with the optimal wavelength for inter-atomic-scale diffraction. However, electrons and neutrons are also common sources, with their frequency determined by their de Broglie wavelength. When these waves reach the sample, the incoming beam is either reflected off the surface, or can enter the lattice and be diffracted by the atoms present in the sample. If the atoms are arranged symmetrically with a separation distance d, these waves will interfere constructively only where the path-length difference 2dsinθ is equal to an integer multiple of the wavelength, producing a diffraction maximum in accordance with Bragg's law. These waves interfere destructively at points between the intersections where the waves are out of phase, and do not lead to bright spots in the diffraction pattern. Because the sample itself is acting as the diffraction grating, this spacing is the [atomic spacing].

The distinction between powder and single crystal diffraction is the degree of texturing in the sample. Single crystals have maximal texturing, and are said to be anisotropic. In contrast, in powder diffraction, every possible crystalline orientation is represented equally in a powdered sample (Figure 5.11), the isotropic case. Powder X-ray diffraction (PXRD) operates under the assumption that the sample is randomly arranged. Therefore, a statistically significant number of each plane of the crystal structure will be in the proper orientation to diffract the X-rays. Therefore, each plane will be represented in the signal. In practice, it is sometimes necessary to rotate the sample orientation to eliminate the effects of texturing and achieve true randomness.

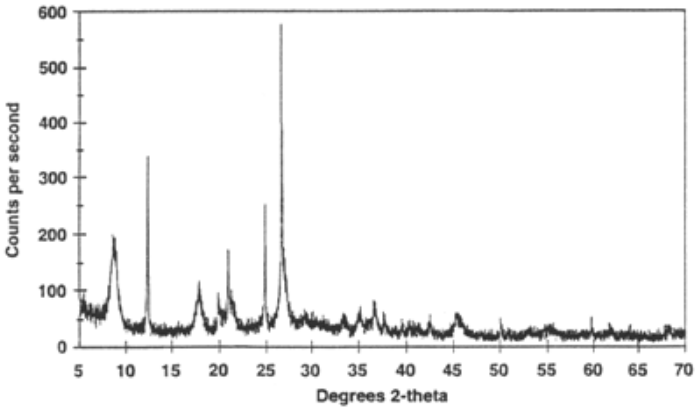

Figure 5.11. X-ray powder diffractogram. Peak positions occur where the X-ray beam has been diffracted by the crystal lattice. The unique set of d-spacings derived from this patter can be used to 'fingerprint' the mineral [112].

This project has been funded with support from the European Commission. This publication [communication] reflects the views only of the authors, and the Commission cannot be held responsible for any use which may be made of the information contained therein.

X-ray powder diffraction is most widely used for the identification of unknown crystalline materials (e.g. minerals, inorganic compounds). Determination of unknown solids is critical to studies in geology, environmental science, material science, engineering and biology.

Other applications include:

- characterization of crystalline materials
- identification of fine-grained minerals such as clays and mixed layer clays that are difficult to determine optically
- determination of unit cell dimensions
- measurement of sample purity

With specialized techniques, XRD can be used to:

- determine crystal structures using Rietveld refinement
- determine of modal amounts of minerals (quantitative analysis)
- characterize thin films samples by:

  - determining lattice mismatch between film and substrate and to inferring stress and strain
  - determining dislocation density and quality of the film by rocking curve measurements
  - measuring superlattices in multilayered epitaxial structures
  - determining the thickness, roughness and density of the film using glancing incidence X-ray reflectivity measurements

- make textural measurements, such as the orientation of grains, in a polycrystalline sample

5.7 X-ray crystallography (XRC)

X-ray crystallography (XRC) is the experimental science determining the atomic and molecular structure of a crystal, in which the crystalline structure causes a beam of incident X-rays to diffract into many specific directions. By measuring the angles and intensities of these diffracted beams, a crystallographer can produce a three-dimensional picture of the density of electrons within the crystal. From this electron density, the mean positions of the atoms in the crystal can be determined, as well as their chemical bonds, their crystallographic disorder, and various other information.

Since many materials can form crystals—such as salts, metals, minerals, semiconductors, as well as various inorganic, organic, and biological molecules—X-ray crystallography has been fundamental in the development of many scientific fields. In its first decades of use, this method determined the size of atoms, the lengths and types of chemical bonds, and the atomic-scale differences among various materials, especially minerals and alloys. The method also revealed the structure and function of many biological molecules, including vitamins, drugs, proteins and nucleic acids such as DNA. X-ray crystallography is still the primary method for characterizing the atomic structure of new materials and in discerning materials that appear similar by other experiments. X-ray crystal structures can also

This project has been funded with support from the European Commission. This publication [communication] reflects the views only of the authors, and the Commission cannot be held responsible for any use which may be made of the information contained therein.

account for unusual electronic or elastic properties of a material, shed light on chemical interactions and processes, or serve as the basis for designing pharmaceuticals against diseases.

In a single-crystal X-ray diffraction measurement, a crystal is mounted on a goniometer. The goniometer is used to position the crystal at selected orientations. The crystal is illuminated with a finely focused monochromatic beam of X-rays, producing a diffraction pattern of regularly spaced spots known as reflections. The two-dimensional images taken at different orientations are converted into a three-dimensional model of the density of electrons within the crystal using the mathematical method of Fourier transforms, combined with chemical data known for the sample. Poor resolution (fuzziness) or even errors may result if the crystals are too small, or not uniform enough in their internal makeup.

X-ray crystallography is related to several other methods for determining atomic structures. Similar diffraction patterns can be produced by scattering electrons or neutrons, which are likewise interpreted by Fourier transformation. If single crystals of sufficient size cannot be obtained, various other X-ray methods can be applied to obtain less detailed information; such methods include fiber diffraction, powder diffraction and (if the sample is not crystallized) small-angle X-ray scattering (SAXS). If the material under investigation is only available in the form of nanocrystalline powders or suffers from poor crystallinity, the methods of electron crystallography can be applied for determining the atomic structure (Figure 5.12).

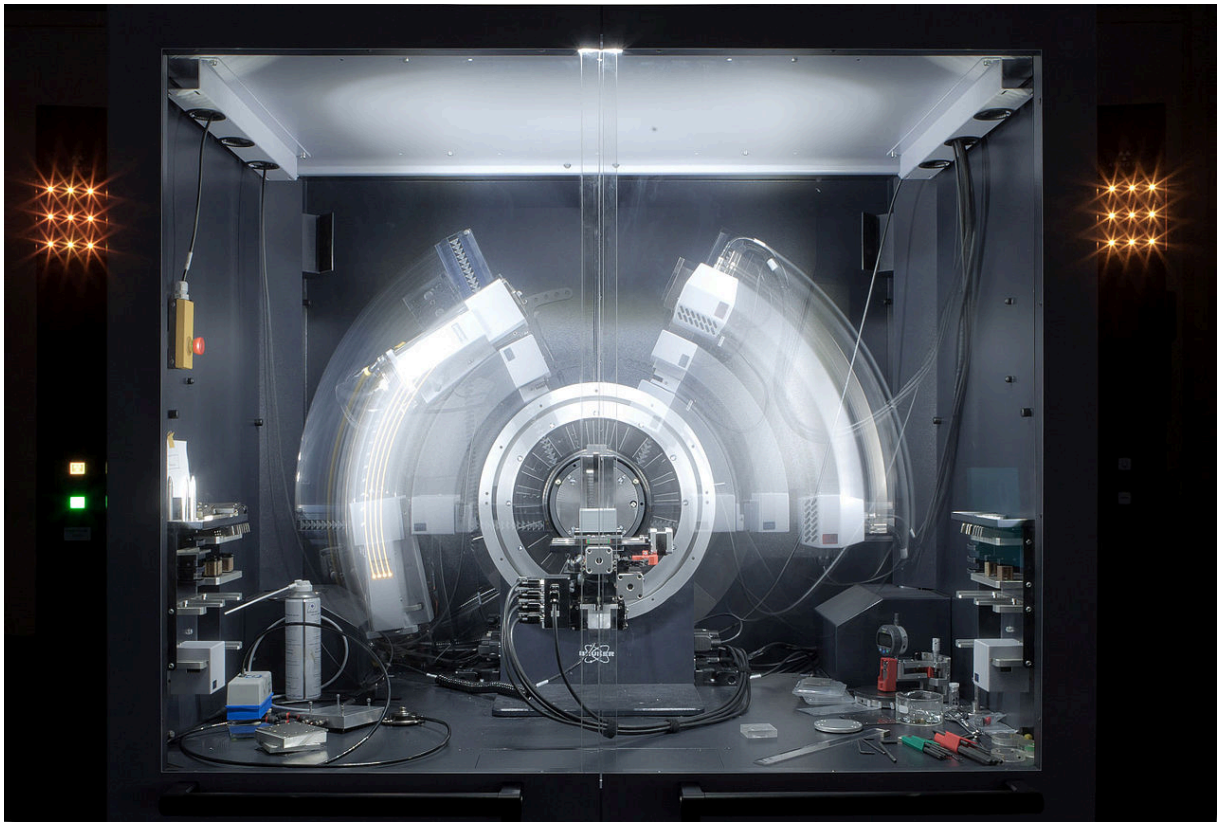

Figure 5.12. A powder X-ray diffractometer in motion [113].

This project has been funded with support from the European Commission. This publication [communication] reflects the views only of the authors, and the Commission cannot be held responsible for any use which may be made of the information contained therein.

For all above mentioned X-ray diffraction methods, the scattering is elastic; the scattered X-rays have the same wavelength as the incoming X-ray. By contrast, inelastic X-ray scattering methods are useful in studying excitations of the sample such as plasmons, crystal-field and orbital excitations, magnons, and phonons, rather than the distribution of its atoms.

The technique of single-crystal X-ray crystallography has three basic steps. The first—and often most difficult—step is to obtain an adequate crystal of the material under study. The crystal should be sufficiently large (typically larger than 0.1 mm in all dimensions), pure in composition and regular in structure, with no significant internal imperfections such as cracks or twinning.

In the second step, the crystal is placed in an intense beam of X-rays, usually of a single wavelength (monochromatic X-rays), producing the regular pattern of reflections. The angles and intensities of diffracted X-rays are measured, with each compound having a unique diffraction pattern. As the crystal is gradually rotated, previous reflections disappear and new ones appear; the intensity of every spot is recorded at every orientation of the crystal. Multiple data sets may have to be collected, with each set covering slightly more than half a full rotation of the crystal and typically containing tens of thousands of reflections.

In the third step, these data are combined computationally with complementary chemical information to produce and refine a model of the arrangement of atoms within the crystal. The final, refined model of the atomic arrangement—now called a crystal structure—is usually stored in a public database (figure 5.13).

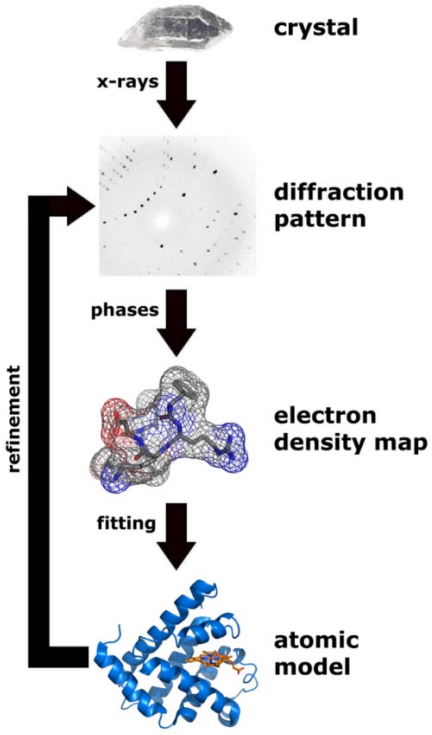

Figure 5.13. Workflow for solving the structure of a molecule by X-ray crystallography [113].

This project has been funded with support from the European Commission. This publication [communication] reflects the views only of the authors, and the Commission cannot be held responsible for any use which may be made of the information contained therein.

6. Summary

The success of an implant depends on the type of biomaterial used for its fabrication. An ideal implant material should be biocompatible, inert, mechanically durable, and easily moldable. The ability to build patient specific implants incorporated with bioactive drugs, cells, and proteins has made 3D printing technology revolutionary in medical and pharmaceutical fields. A vast variety of biomaterials are currently being used in medical 3D printing, including metals, ceramics, polymers, and composites. With continuous research and progress in biomaterials used in 3D printing, there has been a rapid growth in applications of 3D printing in manufacturing customized implants, prostheses, drug delivery devices, and 3D scaffolds for tissue engineering and regenerative medicine. The current review focuses on:

- the novel biomaterials used in variety of 3D printing technologies for clinical applications. Most common types of medical 3D printing technologies, including fused deposition modeling, extrusion based bioprinting, inkjet, and polyjet printing techniques, their clinical applications, different types of biomaterials currently used by researchers, and key limitations are must developed,
- destructive mechanical test,
- nondestructive tests,
- destructive mechanical test of the orthoses and prosthesis.

This project has been funded with support from the European Commission. This publication [communication] reflects the views only of the authors, and the Commission cannot be held responsible for any use which may be made of the information contained therein.

7. References

[1] Deepen Banoriya, Rajesh Purohit, R. K. Dwivedi Modern Trends in Rapid Prototyping for Biomedical Applications. Materials Today: Proceedings 2 (2015) 3409 – 3418.

[2] R. Petzold, H.-F. Zeilhofer, W.A. Kalender, Rapid prototyping technology in medicine-basics and applications, Computerized Medical Imaging and Graphics, Vol. 23, 277-284 (1999).

[3] Rajesh Purohit, and Pramod Sahu, Advances in Rapid Prototyping Technology, Future Trends in Composite Materials and Processing, Vol. 1, 12-14 (2007).

[4] P.A. Webb, A review of rapid prototyping (RP) techniques in the medical and biomedical sector, Journal of Medical Engineering & Technology Vol. 24, 149-153 (2000).

[5] R. Landers, A. Pfister, U. Hu¨Bner, H. John, R. Schmelzeisen, R. Mu¨Lhaupt, Fabrication of soft tissue engineering scaffolds by means of rapid prototyping techniques, Journal of materials science, Vol. 37, 3107-3116 (2002).

[6] Jelena Milovanović, Miroslav Trajanović, Medical applications of rapid prototyping, Mechanical Engineering Vol. 5, 79-85 (2007).

[7] A. Ovsianikov, B. Chichkov, O. Adunka, H. Pillsbury, A. Doraiswamy, R.J. Narayan, Rapid prototyping of ossicular replacement prostheses, Applied Surface Science, Vol. 253, 6603-6607 (2007).

[8] Ferry P.W. Melchels, Jan Feijen, Dirk W. Grijpma, A review on stereolithography and its applications in biomedical engineering, Biomaterials, Vol. 31, 6121-6130 (2010).

[9] Young Joon Seol, Hyun-Wook Kang, Sang Jin Lee, Anthony Atala and James J. Yoo, Bio printing technology and its applications, European Journal of Cardio - Thoracic Surgery, Vol. 46, 342-348 (2014).

[10] Garrett Ryan, Abhay Pandit, Dimitrios Panagiotis Apatsidis, Fabrication methods of porous metals for use in orthopaedic applications, Biomaterials, Vol. 27, 2651-2670 (2006).

[11] Christian Greiner, Scott M. Oppenheimer, David C. Dunand, High strength, low stiffness, porous NiTi with superelastic properties, Acta Biomaterialia, Vol. 1, 705-716 (2005).

[12] Jia Ping Li, Joost R. de Wijn, Clemens A. Van Blitterswijk, Klaas de Groot, Porous Ti6Al4V scaffold directly fabricating by rapid prototyping: Preparation and in vitro experiment, Biomaterials, Vol. 27, 1223-1235 (2006).

[13] Garrett E. Ryan, Abhay S. Pandit, Dimitrios P. Apatsidis, Porous titanium scaffolds fabricated using a rapid prototyping and powder metallurgy technique, Biomaterials, Vol. 29, 3625-3635 (2008).

This project has been funded with support from the European Commission. This publication [communication] reflects the views only of the authors, and the Commission cannot be held responsible for any use which may be made of the information contained therein.

[14] Marco A. Lopez-Heredia, Jerome Sohier, Cedric Gaillard, Sophie Quillard, Michel Dorget, Pierre Layrolle, Rapid prototyped porous titanium coated with calcium phosphate as a scaffold for bone tissue engineering, Biomaterials, Vol. 29, 2608-2615 (2008).

[15] Shoufeng Yang, Kah-Fai Leong, Zhaohui Du, Chee-Kai Chua, The Design of Scaffolds for Use in Tissue Engineering, Part II. Rapid Prototyping Techniques, Tissue Engineering Vol. 8, 1-11(2002).

[16] K.F. Leong, C.M. Cheah, C.K. Chua, Solid freeform fabrication of three-dimensional scaffolds for engineering replacement tissues and organs, Biomaterials, Vol. 24, 2363-2378 (2003).

[17] Guo-Qiang Chen, Qiong Wu, The application of polyhydroxyalkanoates as tissue engineering materials, Biomaterials, Vol. 26, 6565-6578 (2005).

[18] Carlos Mota, Shen-Yu Wang, Dario Puppi, Matteo Gazzarri, Chiara Migone, Federica Chiellini, Guo-Qiang Chen , Emo Chiellini, Additive manufacturing of poly[(R)-3-hydroxybutyrate-co-(R)-3-hydroxyhexanoate] scaffolds for engineered bone development, Journal of Tissue Engineering and Regenerative Medicine, Vol.1, 245-252 (2014).

[19] Ferry P.W. Melchels, Katia Bertoldi, Ruggero Gabbrielli, Aldrik H. Velders, Jan Feijen, Dirk W. Grijpma, Mathematically defined tissue engineering scaffold architectures prepared by stereolithography, Biomaterials, Vol. 31, 6909-6916 (2010).

[20] E.C. Hammel, O.L.R. Ighodaro, O.I.Okolin, Processing and properties of advanced porous ceramics: An application based review, Ceramics International, Vol. 40, 15351-15370 (2014).

[21] Daniel C.N. Chan, Kevin B. Frazier, Laam A. Tse, David W. Rosen, Application of Rapid Prototyping to Operative Dentistry Curriculum, Journal of Dental Education, Vol. 68, 64-70 (2004).

[22] V. N. V. Madhav, Rajendra Daule, Rapid Prototyping and its Application in Dentistry, Journal of Dental & Allied Science, Vol. 2, 57-61 (2013).

[23] Abbas Azari , Sakineh Nikzad, The evolution of rapid prototyping in dentistry: a review, Rapid Prototyping Journal, Vol. 15, 216-225 (2009)

[24] Jean-Jacques Clair, Stereolithography and the biomedical engineering, Journal of Materials Processing Technology, Vol. 57, 393-396 (1996)

[25] Qingbin Liu, Ming C. Leu, Stephen M. Schmitt, Rapid prototyping in dentistry: technology and application, International Journal of Advanced Manufacturing Technology, Vol. 29, 317-335(2006).

This project has been funded with support from the European Commission. This publication [communication] reflects the views only of the authors, and the Commission cannot be held responsible for any use which may be made of the information contained therein.

[26] M. Wu, J. Tinschert, M. Augthun, I. Wagner, J. SchaÈdlich-Stubenrauch, P.R. Sahm, H. Spiekermann, Application of laser measuring, numerical simulation and rapid prototyping to titanium dental castings, Dental Materials,Vol. 17, 102-108 (2001).

[27] Richard Van Noort, The future of dental devices is digital, Dental materials,Vol. 28, 3-12 (2012).

[28] A. Nizam, R.N. Gopal, L. Naing, A.B. Hakim, A.R. Samsudin, Dimensional Accuracy of the Skull Models Produced by Rapid Prototyping Technology Using Stereolithography Apparatus, Archives of Orofacial Sciences, Vol. 1, 60-66 (2006).

[29] Filip Gorski – article under preparing.

Chapter 4.

[30] ISO 17296-3:2014 Additive manufacturing — General principles — Part 3: Main characteristics and corresponding test methods

[31] ISO 2039-1:2001 Plastics — Determination of hardness — Part 1: Ball indentation method

[32] ISO 6507-1:2018 Metallic materials — Vickers hardness test — Part 1: Test method

[33] ISO 14705:2016 Fine ceramics (advanced ceramics, advanced technical ceramics) — Test method for hardness of monolithic ceramics at room temperature

[34] ISO 2039-2:1987 Plastics — Determination of hardness — Part 2: Rockwell hardness

[35] ISO 868:2003 Plastics and ebonite — Determination of indentation hardness by means of a durometer (Shore hardness)

[36] Schmidt Control Instruments website, digital image, accessed 30.05.2021, < https://www.hans-schmidt.com/media/produktansicht-shta-590x481.jpg>.

[37] ISO 6892-1:2019 Metallic materials — Tensile testing — Part 1: Method of test at room temperature

[38] ISO 527-1:2019 Plastics — Determination of tensile properties — Part 1: General principles

[39] ISO 15490:2008 Fine ceramics (advanced ceramics, advanced technical ceramics) — Test method for tensile strength of monolithic ceramics at room temperature

[40] J. R. Davis, Tensile Testing, 2nd Edition, ASM International, 2004, pp. 2

[41] ISO 148-2:2016 Metallic materials — Charpy pendulum impact test — Part 2: Verification of testing machines

[42] ISO 179-2:2020 Plastics — Determination of Charpy impact properties — Part 2: Instrumented impact test

This project has been funded with support from the European Commission. This publication [communication] reflects the views only of the authors, and the Commission cannot be held responsible for any use which may be made of the information contained therein.

[43] ISO 11491:2017 Implants for surgery — Determination of impact resistance of ceramic femoral heads for hip joint prostheses

[44] ISO 180:2000 Plastics — Determination of Izod impact strength

[45] ISO 604:2002 Plastics — Determination of compressive properties

[46] ASTM E9 – 19 Standard Test Methods of Compression Testing of Metallic Materials at Room Temperature

[47] ISO 17162:2014 Fine ceramics (advanced ceramics, advanced technical ceramics) — Mechanical properties of monolithic ceramics at room temperature — Determination of compressive strength

[48] ISO 3327:2009 Hardmetals — Determination of transverse rupture strength

[49] ISO 178:2019 Plastics — Determination of flexural properties

[50] ISO 14704:2008 Fine ceramics (advanced ceramics, advanced technical ceramics) — Test method for flexural strength of monolithic ceramics at room temperature

[51] ISO 1099:2017 Metallic materials — Fatigue testing — Axial force-controlled method

[52] ISO 1143:2010 Metallic materials — Rotating bar bending fatigue testing

[53] ISO 13003:2003 Fibre-reinforced plastics — Determination of fatigue properties under cyclic loading conditions

[54] ISO 15850:2014 Plastics — Determination of tension-tension fatigue crack propagation — Linear elastic fracture mechanics (LEFM) approach

[55] ISO 22214:2006 Fine ceramics (advanced ceramics, advanced technical ceramics) — Test method for cyclic bending fatigue of monolithic ceramics at room temperature

[56] ISO 28704:2011 Fine ceramics (advanced ceramics, advanced technical ceramics) — Test method for cyclic bending fatigue of porous ceramics at room temperature

Chapter 5

[57] Dillner S, Georgiev G. Technical and clinical function testing of hand orthoses in Sweden. Int J Rehabil Res. 1979;2(1):47-60. doi: 10.1097/00004356-197902000-00005. PMID: 478724.

[58] Rogers B, Bosker GW, Crawford RH, et al. Advanced Trans-Tibial Socket Fabrication Using Selective Laser Sintering. Prosthetics and Orthotics International. 2007;31(1):88-100. doi:10.1080/03093640600983923

[59] Jennifer Olsen, Sarah Day, Sigrid Dupan, Kianoush Nazarpour, Matthew Dyson ,3D-Printing and upper-limb prosthetic sockets; promises and pitfalls. bioRxiv 2020.09.21.306050; doi: https://doi.org/10.1101/2020.09.21.306050

This project has been funded with support from the European Commission. This publication [communication] reflects the views only of the authors, and the Commission cannot be held responsible for any use which may be made of the information contained therein.

[60] Yan Wang, Qitao Tan, Fang Pu, David Boone, Ming Zhang. A Review of the Application of Additive Manufacturing in Prosthetic and Orthotic Clinics from a Biomechanical Perspective, Engineering, Volume 6, Issue 11, 2020. https://doi.org/10.1016/j.eng.2020.07.019.

[61] V. Kovan, T. Tezel, H. Camurlu, and E. Topal. Efect of printing parameters on mechanical properties of 3D printed PLA/carbon composites. Materials Science. Non-Equilibrium Phase Transformations.,4(4):126{128, 2018.

[62] International Organization for Standardization, ISO 22523 External limb prostheses and external orthoses, Switzerland: Requirements and test methods, 2006.

[63] R. Mio, M. Sanchez, Q. Valverde, J. Lara, F. Rumiche "Mechanical Testing Methods for Body-Powered Upper-Limb Prostheses: A Case Study", Advances in Science, Technology and Engineering Systems Journal, vol. 4, no. 5, pp. 61-68 (2019).

[64] V. Nagaraja, J. Bergmann, D. Sen and M. Thompson, "Examining the needs of affordable upper limb prosthetic users in India: A questionnaire-based survey," Technology and Disability, vol. 1, pp. 1-10, 2016.

[65] M. Vergara, J. Sancho, V. Gracia and A. Pérez, "An introductory study of common grasps used by adults during performance of activities of daily living," Journal of Hand Therapy, vol. 27, pp. 225-234, 2014.

[66] Cuellar JS, Smit G, Breedveld P, Zadpoor AA, Plettenburg D. Functional evaluation of a non-assembly 3D-printed hand prosthesis. Proc Inst Mech Eng H. 2019 Nov;233(11):1122-1131. doi: 10.1177/0954411919874523. Epub 2019 Sep 6. PMID: 31597553; PMCID: PMC6790990.

[67] Mercado, Abimael, Aung Heain Soe, Sean Greene, and Daniel Evan Lipson. 2016. Design And Manufacture Of A Scalable Prosthetic Hand Through The Utilization Of Additive Manufacturing. : Worcester Polytechnic Institute.

[68] A. McGarry, B. McHugh, J. Duers, and A. W. Buis. Design of manikin for testing of residual-limbshape-capture method. Journal of Rehabilitation Research & Development, 48(3):245, 2011

[69] Manero A, Smith P, Sparkman J, et al. Implementation of 3D Printing Technology in the Field of Prosthetics: Past, Present, and Future. Int J Environ Res Public Health. 2019;16(9):1641. Published 2019 May 10. doi:10.3390/ijerph16091641

[70] American Orthotic & Prosthetic Association. AOPA's Prosthetic Foot Project: What it is, what it is not, and what patient care facility providers/practitioners need to know [Internet]. Alexandria (VA): American Orthotic & Prosthetic Association; 2010. Available from: https://www.aopanet.org/wp-content/uploads/2013/12/Prosthetic_Foot_Project.pdf

[71] Major MJ, Johnson WB, Gard SA. Interrater reliability of mechanical tests for functional classification of transtibial prosthesis components distal to the socket. J Rehabil Res Dev. 2015;52(4):467-76. doi: 10.1682/JRRD.2014.12.0300. PMID: 26360815.

[72] Rochlitz, B., Pammer, D. "Design and Analysis of 3D Printable Foot Prosthesis", Periodica Polytechnica Mechanical Engineering, 61(4), pp. 282-287, 2017. https://doi.org/10.3311/PPme.11085

This project has been funded with support from the European Commission. This publication [communication] reflects the views only of the authors, and the Commission cannot be held responsible for any use which may be made of the information contained therein.

[73] Porras, F., Araya, M., Sánchez, O., Vargas, R., & Corrales, S. (2020). Structural Static Characterization of a Novel 3D Printed Prosthetic Foot. Transactions on Additive Manufacturing Meets Medicine, 2(1). https://doi.org/10.18416/AMMM.2020.2009009

[74] ISO 22675:2016 Prosthetics — Testing of ankle-foot devices and foot units — Requirements and test methods

[75] Trotta T, Trotta J, Lowe S. Human tissue models, materials, and methods. United States patent US 20130192741A1 2013.

[76] Shane D. Curry, Thomas C. Pond, Emma K. Vogan, Gabrielle E. Griffith, Jared R. Rider. Mechanical Testing of 3D Printed Prosthetics. 2020 COLLABORATORY / ENGINEERING SYMPOSIUM

[77] Stenvall E, Flodberg G, Pettersson H, Hellberg K, Hermansson L, Wallin M, Yang L. Additive Manufacturing of Prostheses Using Forest-Based Composites. Bioengineering. 2020; 7(3):103. https://doi.org/10.3390/bioengineering7030103

[78] ISO 10328:2016 Prosthetics — Structural testing of lower-limb prostheses — Requirements and test methods

[79] Ryan Schmidt, ginger coons, Vincent Chen, Timotheius Gmeiner, and Matt Ratto. 2015. 3D-printed prosthetics for the developing world. In SIGGRAPH 2015: Studio (SIGGRAPH '15). Association for Computing Machinery, New York, NY, USA, Article 21, 1. DOI:https://doi.org/10.1145/2785585.2792535

[80] Quinlan J, Yohay J, Subramanian V, Poziembo B, Fatone S. Using mechanical testing to assess the effect of lower-limb prosthetic socket texturing on longitudinal suspension. PLoS One. 2020 Aug 19;15(8):e0237841. doi: 10.1371/journal.pone.0237841. PMID: 32813733; PMCID: PMC7437898.

[81] Wähnert D, Hoffmeier KL, Stolarczyk Y, Fröber R, Hofmann GO, Mückley T. Evaluation of a Customized Artificial Osteoporotic Bone Model of the Distal Femur. Journal of Biomaterials Applications. 2011;26(4):451-464. doi:10.1177/0885328210367830

[82] Cagle JC, Reinhall PG, Hafner BJ, Sanders JE. Development of Standardized Material Testing Protocols for Prosthetic Liners. J Biomech Eng. 2017 Apr 1;139(4):0450011–04500112. doi: 10.1115/1.4035917. PMID: 28233885; PMCID: PMC5444209.

[83] T. Ramakrishnan, M. Schlafly and K. B. Reed, "Evaluation of 3D printed anatomically scalable transfemoral prosthetic knee," 2017 International Conference on Rehabilitation Robotics (ICORR), 2017, pp. 1160-1164, doi: 10.1109/ICORR.2017.8009406.

[84] Nietert, M.; Englisch, N.; Kreil, P.; Alba-lopez, G. Loads in hip disarticulation prostheses during normal daily use, Prosthetics and Orthotics International: December 1998 - Volume 22 - Issue 3 - p 199-215 doi: 10.3109/03093649809164485

[85] ISO 15032:2000 Prostheses — Structural testing of hip units

[86] Wu J., Zhao C., Liu Y., Ma S. (2018) Mechanical Analysis of a Customized Hand Orthosis Based on 3D printing. In: Wang K., Wang Y., Strandhagen J., Yu T. (eds) Advanced Manufacturing and Automation VII. IWAMA 2017. Lecture Notes in Electrical Engineering, vol 451. Springer, Singapore. https://doi.org/10.1007/978-981-10-5768-7_53

This project has been funded with support from the European Commission. This publication [communication] reflects the views only of the authors, and the Commission cannot be held responsible for any use which may be made of the information contained therein.

[87] Luca Toth, Adam Schiffer, Miklos Nyitrai, Attila Pentek, Roland Told, Peter Maroti, Developing an anti-spastic orthosis for daily home-use of stroke patients using smart memory alloys and 3D printing technologies, Materials & Design, Volume 195, 2020,https://doi.org/10.1016/j.matdes.2020.109029.

[88] ISO 32100:2018 Rubber- or plastics-coated fabrics — Physical and mechanical tests — Determination of flex resistance by the flexometer method

[89] Górski, F.; Wichniarek, R.; Kuczko, W.; Żukowska, M.; Lulkiewicz, M.; Zawadzki, P. Experimental Studies on 3D Printing of Automatically Designed Customized Wrist-Hand Orthoses. Materials 2020, 13, 4091. https://doi.org/10.3390/ma13184091

[90] International Organization for Standardization. ISO 527-2:2012. In Plastics—Determination of Tensile Properties—Part 2: Test Conditions for Moulding and Extrusion Plastics; International Organization forStandardization: Geneva, Switzerland, 2012.

[91] Kuang-Wei Lin, Chia-Jung Hu, Wen-Wen Yang, Li-Wei Chou, Shun-Hwa Wei, Chen-Sheng Chen, Pi-Chang Sun, "Biomechanical Evaluation and Strength Test of 3D-Printed Foot Orthoses", Applied Bionics and Biomechanics, vol. 2019, Article ID 4989534, 8 pages, 2019. https://doi.org/10.1155/2019/4989534

[92] Hochmann, D. 2014. Testing Procedures for Ancle-Foot Orthoses. Orthotics. Special edition from Orthopadie Technik 5/14:1-4. Online: https://verlag-ot.de/content/e3741823/e3763487/e3763729/e3763737/tiles3763742/tileElements3763743/1310_SD_Hochmann_5_14_OB_GB_ger.pdf

[93] Chin, R.; Hsiao-Wecksler, E. T.; Loth, E.; Kogler, G.F.; Manwaring, S. D.; Tyson, S. N.; Shorter, K.A.; Gilmer, J. N. et al. 2009. A pneumatic power harvest-ing ankle-foot orthosis to prevent foot-drop. Journal of NeuroEngineering and Rehabilitation 6:19. http://dx.doi.org/10.1186/1743-0003-6-19.

[94] Zou, D.; He, T.; Dailey, M.; Smith, K. E.;Silva, M. J.; Sinacore, D. R.; Mueller, M. J.; Hastings, M. K. 2014. Experimental and computational analysis of composite ankle-foot orthosis. J Rehabil Res Dev 51(10): 1525-36. http://dx.doi.org/10.1682/JRRD.2014-02-0046

[95] Mavroidis, C.; Ranky, R. G.; Sivak, M. L.; Patritti, B. L.; DiPisa, J.; Caddle, A.; Gilhooly, K.; Govoni, L.; Sivak, S.; Lancia, M.; Drillio, R.; Bonato, P. 2011. Patient specific ankle-foot orthoses using rapid proto-typing. Journal of NeuroEngineering and Rehabilitation8: 1.

[96] Griskevicius, J., Daunoraviciene, K., Krukonis, K., & Kilikevičius, A. (2017). Method for ankle foot orthotics' mechanical assessment: a pilot study.

[97] Sheehan C, Figgins E. A comparison of mechanical properties between different percentage layups of a single-style carbon fibre ankle foot orthosis. Prosthetics and Orthotics International. 2017;41(4):364-372. doi:10.1177/0309364616652015

[98] BS EN ISO 22675:2006 . Prosthetics: testing of ankle-foot devices and foot units – requirements and test methods.

[99] Lin, Y.-C.; Huang, L.-Y.; Chen, C.-S. Strength Evaluation and Modification of a 3D Printed Anterior Ankle Foot Orthoses. Appl. Sci. 2020, 10, 7289. https://doi.org/10.3390/app10207289

This project has been funded with support from the European Commission. This publication [communication] reflects the views only of the authors, and the Commission cannot be held responsible for any use which may be made of the information contained therein.

[100] Cha YH, Lee KH, Ryu HJ, Joo IW, Seo A, Kim DH, Kim SJ. Ankle-Foot orthosis Made by 3D Printing Technique and Automated Design Software. Appl Bionics Biomech. 2017;2017:9610468. doi: 10.1155/2017/9610468. Epub 2017 Jul 30. PMID: 28827977; PMCID: PMC5554564.

[101] JENSEN, W. A., AND R. B. PARK. Cell ultrastructure. Wadsworth Publishing Company, Inc., Belmont, California. 1967, 60 p.

[102] F. OHNESORGE AND G. BINNIG: True Atomic Resolution by Atomic Force Microscopy Through Repulsive and Attractive Forces, SCIENCE, Vol 260, Issue 5113, pp. 1451-1456, 1993

[103] Giessibl, Franz "Atomic Resolution of the Silicon (111)-(7x7) Surface by Atomic Force Microscopy" (PDF). Science. 267 (5194): 68–71. doi:10.1126/science.267.5194.68. PMID 17840059. S2CID 20978364, 1.01.1996

[104] R Sri Muthu Mrinalini & G R Jayanth, Atomic Force Microscopes get a technology boost. 2016. Retrived from: https://indianexpress.com

[105] Atomic force microscopy, Wikipedia, 2015. https://en.wikipedia.org/wiki/Atomic_force_microscopy

[106] Microscopiu electrónicu, Wikipedia Spain, 2007. https://ast.wikipedia.org/wiki/Microscopiu_electr%C3%B3nicu

[107] Mikroskop tem, Pik instruments. https://mikroskopelektronowy.pl/mikroskop-tem/

[108] VHX-7000 Series Digital Microscope Catalogue, Keyence. https://www.keyence.eu/landing/lpc/1812-vh-measuring-microscope.jsp

[109] Optical microscope, Wikipedia, 2007. https://en.wikipedia.org/wiki/Optical_microscope

[110] Joseph Goldstein: Scanning Electron Microscopy and X-Ray Microanalysis. Springer. ISBN 978-0-306-47292-3. Retrieved 26 May 2012.

[111] Energy-dispersive X-ray spectroscopy, Wikipedia, 2009. https://en.wikipedia.org/wiki/Energy-dispersive_X-ray_spectroscopy

[112] M. J. K. Flohr, X-Ray powder diffraction, U.S. Geological Survey, 2007. https://pubs.usgs.gov/info/diffraction/xrd.pdf

[113] X-ray crystallography, Wikipedia, 2015. https://en.wikipedia.org/wiki/X-ray_crystallography

This project has been funded with support from the European Commission. This publication [communication] reflects the views only of the authors, and the Commission cannot be held responsible for any use which may be made of the information contained therein.

7 Summary

The success of an implant depends on the type of biomaterial used for its fabrication. An ideal implant material should be biocompatible, inert, mechanically durable, and easily moldable. The ability to build patient specific implants incorporated with bioactive drugs, cells, and proteins has made 3D printing technology revolutionary in medical and pharmaceutical fields. A vast variety of biomaterials are currently being used in medical 3D printing, including metals, ceramics, polymers, and composites. With continuous research and progress in biomaterials used in 3D printing, there has been a rapid growth in applications of 3D printing in manufacturing customized implants, prostheses, drug delivery devices, and 3D scaffolds for tissue engineering and regenerative medicine. The current review focuses on:

- the novel biomaterials used in variety of 3D printing technologies for clinical applications. Most common types of medical 3D printing technologies, including fused deposition modeling, extrusion based bioprinting, inkjet, and polyjet printing techniques, their clinical applications, different types of biomaterials currently used by researchers, and key limitations are must developed,
- destructive mechanical test,
- nondestructive tests,
- destructive mechanical test of the orthoses and prothesis.

This project has been funded with support from the European Commission. This publication [communication] reflects the views only of the authors, and the Commission cannot be held responsible for any use which may be made of the information contained therein.

[1] Fig. 4.1 - JENSEN, W. A., AND R. B. PARK. Cell ultrastructure. Wadsworth Publishing Company, Inc., Belmont, California. 1967, 60 p.

[2] F. OHNESORGE AND G. BINNIG: True Atomic Resolution by Atomic Force Microscopy Through Repulsive and Attractive Forces, SCIENCE, Vol 260, Issue 5113, pp. 1451-1456, 1993

[3] Giessibl, Franz "Atomic Resolution of the Silicon (111)-(7x7) Surface by Atomic Force Microscopy" (PDF). Science. 267 (5194): 68–71. doi:10.1126/science.267.5194.68. PMID 17840059. S2CID 20978364, 1.01.1996

[4] Joseph Goldstein: Scanning Electron Microscopy and X-Ray Microanalysis. Springer. ISBN 978-0-306-47292-3. Retrieved 26 May 2012.

This project has been funded with support from the European Commission. This publication [communication] reflects the views only of the authors, and the Commission cannot be held responsible for any use which may be made of the information contained therein.

This project has been funded with support from the European Commission. This publication [communication] reflects the views only of the authors, and the Commission cannot be held responsible for any use which may be made of the information contained therein.